Brain inflammation induces post-synaptic changes during early synapse formation in adult-born hippocampal neurons.

Chugh, Deepti; Nilsson, Per; Afjei, Seyedeh Atiyeh; Bakochi, Anahita; Ekdahl Clementson, Christine

Published in:
Experimental Neurology

DOI:
10.1016/j.expneurol.2013.09.005

2013

Brain Inflammation Induces Post-Synaptic Changes During Early Synapse Formation in Adult-Born Hippocampal Neurons

Deepti Chugh[1,2], Per Nilsson[1], Seyedeh-Atiyeh Afjei[1], Anahita Bakochi[1], Christine T Ekdahl[1,2]

[1]Inflammation and Stem Cell Therapy Group, Wallenberg Neuroscience Center, Division of Clinical Neurophysiology, Lund University, SE-221 84 Lund, Sweden

[2]Epilepsy Center, Department of Clinical Sciences, Lund University, SE-221 84 Lund, Sweden

Abbreviated title: Inflammation and Synaptic Adhesion during Neurogenesis

Corresponding author:
Christine T Ekdahl MD PhD
Inflammation and Stem Cell Therapy Group, Wallenberg Neuroscience Center, Division of Clinical Neurophysiology, Lund University and Skåne University Hospital, SE-221 84 Lund, Sweden
Telephone: +46-46-2220550
Fax: +46-46-2220560
Email: Christine.Ekdahl_Clementson@med.lu.se

Number of pages: 46
Number of figures: 7

Abstract

An inflammatory reaction in the brain is primarily characterized by activation of parenchymal microglial cells. **Microglia regulate several aspects of adult neurogenesis, i.e. the continuous production of new neurons in the adult brain. Hippocampal neurogenesis is thought to be important for memory formation, but its role in brain diseases is not clear. We have previously shown that brain inflammation** modulates the functional integration of newly formed hippocampal neurons. **Here, we explored whether there is a defined time period during synaptic development when new neurons are susceptible to brain inflammation. N**ewly formed **hippocampal** neurons, born in an intact environment in the adult mouse brain, **were exposed to** lipopolysaccharide (LPS)-induced inflammation during either early or late phases of **excitatory and inhibitory** synaptogenesis. **We used intra-hippocampal injections of** GFP-retroviral vector (RV-GFP) **to label the new neurons** and ipsilateral LPS injection at either 1 or 4 weeks post-RV-GFP injection. A single intra-hippocampal LPS injection induced an inflammatory response for at least 3 weeks, including an acute transient pro-inflammatory cytokine release as well as a sub-acute and sustained change in microglial morphology. **The general cytoarchitecture of the hippocampal dentate gyrus, including granule cell layer (GCL) volume, and astrocytic glial fibrillary acidic protein expression were not different compared to vehicle controls, and no Fluoro-Jade-positive cell death was observed.** New neurons encountering this inflammatory environment exhibited no changes in their gross morphology. However, **when inflammation occurred during** early stages of synapse formation, we found a region-specific increase in the number of thin dendritic spines and post-synaptic density-95 (PSD-95) cluster formation on spines, suggesting an enhanced excitatory synaptic connectivity

in the newborn neurons. **No changes were observed in the expression of N-cadherin, an adhesion molecule primarily associated with excitatory synapses. At the inhibitory synapses, alterations due to inflammation were also evident** during early but not later stages of synaptic development. Gephyrin, an inhibitory scaffolding protein, was down-regulated in the somatic region, while the adhesion molecules **neuroligin-2 (NL-2) and neurofascin** were increased in the somatic region and/or on the dendrites**. The $GABA_A$ receptor-α2 subunit ($GABA_AR$-α2) was increased, while pre/peri-synaptic GABA clustering remained unaltered. The disproportional changes in post-synaptic adhesion molecules and $GABA_A$ receptor compared to scaffolding protein expression at the inhibitory synapses during brain inflammation are likely to cause an imbalance in GABAergic transmission. These changes were specific for the newborn neurons and were not observed when estimating the overall expression of gephyrin, NL-2, and $GABA_AR$-α2 in the hippocampal GCL. The expression of** interleukin-1-type 1 receptor (IL-1R1) on preferentially the somatic region **of new neurons, often** in close apposition to NL-2 clusters, **may indicate a direct interaction between brain inflammation and synaptic proteins on newborn neurons. In summary,** this study provides evidence that adult-born hippocampal neurons alter their **inhibitory and excitatory** synaptic integration when encountering an LPS-induced brain inflammation during the initial stages of synapse formation. **Changes at this critical developmental period are likely to interfere with the physiological functions of new neurons within the hippocampus.**

Keywords

Lipopolysaccharide; inflammation; microglia; hippocampus; neurogenesis; adhesion molecules

Introduction

The adult mammalian brain is endowed with the capacity to produce new neurons throughout the lifetime of an organism. This phenomenon of adult neurogenesis is restricted to two brain regions; the subventricular zone lining the lateral ventricles and the subgranular zone (SGZ) of the hippocampal dentate gyrus **(Curtis, et al., 2007, Eriksson, et al., 1998,** Zhao, et al., 2008). The newly formed neurons integrate into the adult neuronal circuitry of the olfactory bulb and hippocampus as interneurons and granule cells, respectively. **In humans, the annual turnover of hippocampal granule cells has been estimated to be 1.75% (Spalding, et al., 2013) and according to animal studies they may contribute to memory formation (Gu, et al., 2012, Kee, et al., 2007). However, their role during brain diseases is not clear.** Various pathological insults, including epileptic seizures and stroke, modulate different aspects of adult neurogenesis, ranging from cell proliferation, migration, differentiation, survival, and subsequently functional integration (Arvidsson, et al., 2002, Bengzon, et al., 1997, Ekdahl, et al., 2001, Jakubs, et al., 2006, Parent, et al., 1997). One of the hallmarks of these brain pathologies is neuroinflammation, which primarily involves innate immune signaling through activation of parenchymal microglial cells (Danton and Dietrich, 2003, Gorter, et al., 2006), but also an adaptive immune response with the recruitment of systemic immune cells (Mosley, et al., 2012, Shichita, et al., 2009, Wraith and Nicholson, 2012).

Lipopolysaccharide (LPS) is an endotoxin of gram-negative bacteria, used extensively for inducing an immune response in the brain both through peripheral

(Laflamme, et al., 2003) and intra-cerebral administration (Deng, et al., 2012, Herber, et al., 2006, Zhou, et al., 2012). LPS-induced microglial activation in the brain can be characterized by an increase in the proliferation and migration of the cells, as well as changes in their expression / secretion of inflammatory mediators. However, several studies have stressed the dual role of activation, by which the microglia may exert both detrimental / neurodamaging and beneficial / neuroprotective effects, possibly through differential expression of pro- (i.e. interleukin (IL) -1β, IL-6 or tumor necrosis factor (TNF)-α) and anti- (i.e. IL-4, IL-10 or transforming growth factor (TGF)-β) inflammatory cytokines, respectively (Nguyen, et al., 2002). Consistently, there is accumulating evidence suggesting that microglial activation may simultaneously or sequentially both promote and prohibit adult neurogenesis, depending on the activation stage and the functional balance of secreted molecules with pro- and anti-inflammatory action (Butovsky, et al., 2006, Ekdahl, et al., 2003, Ekdahl, et al., 2009, Monje, et al., 2003). Most of these studies have focused on the initial stages of neurogenesis including proliferation, survival and neuronal fate determination. The role of microglia at later stages, i.e., during synaptic assembly, stability, and transmission, is just beginning to be unraveled (Ekdahl, 2012).

Adhesion molecules are one of the potential candidates linking the microglial cells to the synaptic integration of adult-born neurons. They are crucial not only during synaptic assembly and development but also in fine-tuning the synaptic response (Arikkath and Reichardt, 2008, Dalva, et al., 2007, Washbourne, et al., 2004). We have previously shown that the expression of Neuroligin-2 (NL-2), an adhesion molecule primarily associated with inhibitory synapses, together with the post-synaptic scaffolding protein gephyrin are significantly altered on newly formed hippocampal neurons in a model of partial *status epilepticus* (SE) (Jackson, et al.,

2012). Interestingly, inflammatory mediators are suggested to regulate the expression of adhesion molecules either directly or indirectly. In fact, N-cadherin, an adhesion molecule present at excitatory synapses is modulated by TNF-α (Kubota, et al., 2009). Additionally, IL-1 receptor accessory protein (IL-1RAcP), an essential component mediating IL-1 cytokine-related immune responses, can itself act as a trans-synaptic cell adhesion molecule in neurons and organize synapse formation (Yoshida, et al., 2012). These studies indicate that adhesion molecules may function as one of the important players in potential signaling pathways between microglia and neurons.

The objectives of the present study was, first, to describe the temporal development of the inflammatory response in the hippocampal dentate gyrus following a single intra-hippocampal LPS injection and, secondly, to analyze the expression of synaptic adhesion molecules and scaffolding proteins related to excitatory and inhibitory transmission on newly formed hippocampal neurons encountering the LPS-induced inflammation during either early or late phase of synaptic development.

Materials and Methods

Animals and group assignment

In total, ninety-eight adult male C57BL/6 mice (Charles Rivers), weighing 25 g each at the beginning of the experiments, were used. The mice were housed under a constant 12 h light/dark cycle with access to food and water *ad libitum*. All experimental procedures followed guidelines set by the Malmö-Lund Ethical Committee for the use and care of laboratory animals.

The animals were included in the following three sets of experiments: Experiment 1: Fifteen mice were used to optimize the intra-hippocampal LPS injections in order to achieve sustained microglial activation throughout the unilateral hippocampal dentate gyrus. This included two different doses of LPS (0.5μl of 0.5 or 1μg/μl) and two different stereotaxic coordinates at 2 survival time points (3 days and 3 weeks). Experiment 2: Eighty-three mice were used for histological (n=47, including mice used in experiment 3) and biochemical (n=36) characterization of LPS-induced inflammation in the ipsilateral hippocampal dentate gyrus. The mice received a single intra-hippocampal injection of LPS or vehicle and were then perfused at three different time points (12 hours, 3 days and 3 weeks). Experiment 3: Thirty-three mice were used for evaluation of synaptic protein expression on newly formed hippocampal neurons following intra-hippocampal LPS injections. These mice first received a stereotaxic injection of green fluorescent protein-expressing retroviral vector (RV-GFP) in the hippocampal dentate gyrus. One or four weeks later, LPS or vehicle was injected into the ipsilateral hippocampus. The mice were then perfused 3 weeks later (at 28 days post-injection (dpi) of RV-GFP and 49 dpi, respectively) for immunohistochemical and confocal analyses.

Lipopolysaccharide (LPS) administration

Animals were anaesthetized with isofluorane (1%) and LPS from *Salmonella enterica*, serotype *abortus equi* (Sigma-Aldrich, Sweden; 0.5 μg in 0.5 μl of artificial CSF (aCSF)) or vehicle (0.5 μl of aCSF) was stereotaxically injected into the left dorsal hippocampus (coordinates: 3.0 mm caudal and 2.5 mm lateral to bregma, and 1.9 mm ventral to dura; toothbar set at -2.2 mm) (Paxinos and Watson, 1997) using a glass microcapillary.

Labeling of new neurons

Animals were anaesthetized with isofluorane (1%) and were stereotaxically injected with 1.5 μl of retroviral vector, containing the GFP gene under the CAG promoter ($4.8*10^8$ TU/ml), unilaterally into the left dorsal hippocampus (coordinates: 2.0 mm caudal and 1.5 mm lateral to bregma, and 1.8 mm ventral to dura; toothbar set at -2.2 mm) using a glass microcapillary (similar to (Laplagne, et al., 2006)).

Enzyme-linked immunosorbent assay (ELISA)

At 12 hours, 3 days and 3 weeks after intra-hippocampal LPS or vehicle injection, mice received an overdose of sodium pentobarbital (200 mg/kg, i.p.) and were trans-cardially perfused with ice-cold saline and whole hippocampus, ipsilateral to the LPS or vehicle injection, was rapidly removed and quickly frozen on dry ice. Samples were homogenized on ice in buffer (pH 7.6), containing (in mM): 50.0 Tris-HCl, 150 NaCl, 5.0 $CaCl_2$, 0.02% NaN_3, 1% Triton X-100, and then centrifuged at 17,000 times gravity for 30 min at 4°C. Protein concentration was determined in supernatants by BCA protein assay as per manufacturer's instructions (Pierce, USA). IL-1β, IL-6, IL-4, and IL-10 concentrations were determined by ELISA (Duoset; R & D Systems, USA) according to manufacturer's protocol.

Immunohistochemistry

For histological analyses, mice were given an overdose of sodium pentobarbital and were trans-cardially perfused with ice-cold saline and paraformaldehyde (PFA) (4% in 0.1 M phosphate buffered saline (PBS), pH 7.4). Brains were removed, post-fixed

overnight, dehydrated in 20% sucrose in 0.1 M PBS overnight, and then cut into 30 μm-thick coronal sections and stored in cryoprotective solution at -20°C until use.

For immunohistochemistry, the following primary antibodies were used: Rabbit anti-Iba1 (1:1000, Wako, Japan), rat anti-CD68/ED1 (1:500, AbD Serotech, Germany), mouse anti- glial fibrillary acidic protein (GFAP) (1:400, Sigma-Aldrich), rabbit anti-GFP (1:5000, Abcam, UK), mouse anti-gephyrin (1:500, Synaptic Systems, Germany), mouse anti-postsynaptic density-95 (PSD-95) (1:200, Abcam), rabbit anti-N-cadherin (1:200, Millipore, Germany), goat anti-neuroligin-2 (NL-2) (1:100, Santa Cruz Biotechnology, Germany), rabbit anti-neurofascin (1:500, Abcam), rabbit anti-gamma amino butyric acid (GABA) (1:2000, Sigma-Aldrich), **rabbit anti-interleukin-1 type-1 receptor (IL-1R1) (1:100, Santa Cruz Biotechnology) and rabbit anti-$GABA_A$ receptor-α2 subunit ($GABA_AR$-α2) (1:1000, Synaptic Systems).** Free-floating sections were incubated with the appropriate primary antibody overnight at 4°C and secondary antibody for 2 h at room temperature. Staining for the synaptic proteins, including adhesion molecules, scaffolding proteins, GABA, **and $GABA_AR$-α2** involved an additional antigen retrieval step with incubation of the sections in sodium citrate buffer (10 mM sodium citrate, 0.05% Tween-20, pH 6) at 90°C for 20 min. Secondary antibodies were: Cy3-conjugated donkey anti-mouse/goat/rat (1:200, Jackson Immunoresearch, UK), Cy3-conjugated goat anti-rabbit (1:200, Jackson Immunoresearch), FITC-conjugated goat anti-rabbit (1:200, Jackson Immunoresearch), Alexa-488 conjugated streptavidin (1:200, Invitrogen, Sweden), or biotinylated goat anti-rabbit/chicken (1:200, Vector laboratories, UK). Sections were mounted on gelatin-coated glass microscopic slides and coverslipped with glycerol-based mounting medium (DABCO, Sigma-Aldrich).

Cresyl violet staining

Brain sections were mounted on gelatin-coated glass microscopic slides, hydrated, rinsed in distilled water, immersed in 0.5% cresyl violet solution, and rinsed again in distilled water. The slides were then dehydrated, immersed in xylene, and coverslipped with Pertex mounting medium (Histolab, Sweden).

Fluoro-Jade staining

Free-floating brain sections were mounted in potassium PBS (KPBS) onto glass microscopic slides and allowed to dry overnight. The procedure used has been described elsewhere (Schmued, et al., 1997). Briefly, the sections were rehydrated, pretreated in 0.06% potassium permanganate for 15 min, rinsed in distilled water, incubated in 0.001% Fluoro-Jade working solution (Histo-Chem, Jefferson, AR, USA) for 30 min, rinsed in distilled water, immersed in xylene, and coverslipped with Pertex mounting medium.

Epifluorescence microscopy

All analyses were conducted by researchers blind to the treatment conditions. Quantification of microglial activation in terms of cell counts and morphology was performed ipsilateral to the LPS or vehicle injection in 3-5 hippocampal sections (from -1.46 mm to -2.46 mm posterior to bregma) as previously described (Jakubs, et al., 2008, Thored, et al., 2009) using an Olympus BX61 epifluorescence microscope. The number of $Iba1^+/ED1^+$ cells was counted in the **entire** molecular layer (ML), granule cell layer (GCL)/SGZ and dentate hilus. **The data is expressed as number of $Iba1^+/ED1^+$ cells per section, based on the average number of $Iba1^+/ED1^+$ cells in 3-5 sections (Ekdahl, et al., 2003, Jakubs, et al., 2008, Wood, et al., 2011).** For

morphological analysis, a total number of 90 Iba1$^+$ cells were analyzed in the ML, and 60 Iba1$^+$ cells were analyzed in the GCL/SGZ and the hilus, respectively. The morphological phenotype of Iba1$^+$ cells was classified into three different subtypes; ramified, intermediate and round/amoeboid. The relative occurrence of each subtype was expressed as the mean percentage of the total number of Iba1$^+$ microglia per animal for each region of interest (ROI).

The cytoarchitecture of the hippocampal dentate gyrus was qualitatively evaluated with respect to cell layer dispersion or destruction in cresyl violet staining, using an Olympus BX61 epifluorescence microscope under 10 X objective. The volume of the GCL was calculated by delineating the boundaries of the GCL in 4 hippocampal sections per animal (from -1.46 mm to -2.46 mm posterior to bregma) to measure the area in each section with the CellSens Dimension software (Olympus). This value was then multiplied with section thickness (0.03 mm), number of sections (n=4), and number of section series (n=8).

Quantification of GFAP staining was performed by intensity measurements. **Fluorescence images engaging representative part of the GCL, ML and dentate hilus, ipsilateral to the LPS or vehicle injection, were acquired from 3-4 hippocampal sections (from -1.46 mm to -2.46 mm posterior to bregma) per animal using an epifluorescence microscope.** The images were then imported in ImageJ software (NIH, USA) and converted to 32-bit grayscale images. Background intensity was measured from the cortex for GFAP, where there was very little positive signal. This value was then subtracted from the mean gray value from each of the ROIs in order to obtain a background-corrected mean gray value per animal.

Gross morphology of newly formed hippocampal neurons was analyzed as described before (Jakubs, et al., 2008). GFP^+ cells were **manually** counted in SGZ/GCL and dentate hilus for analysis of **cell number and** relative distribution of cell bodies in these areas. For all GFP^+ cells, axon exit points, dendritic exit points, and total number of dendrites leaving the cell soma were analyzed. Dendritic polarity was determined by classifying the angle of the dendrites leaving the cell soma as 0-22°, 22.5-67°, or 67.5-90°, where 90° was perpendicular to the GCL.

Confocal microscopy and ImageJ analysis

Dendritic spines and expression of different synaptic proteins (adhesion molecules, scaffolding proteins, GABA, **$GABA_AR$-α2) and IL-1R1** onto the newly formed neurons were evaluated using confocal microscopy as previously described (Jackson, et al., 2012). All images were acquired using a confocal laser scanning microscope (Leica), with Kr-Ar 488 and 568 nm excitation filters, 63 X water immersion objective, and 16 X digital zoom. For dendritic analysis, a total of 12 images were acquired per animal. Images were taken on the proximal and distal part of apical dendrites of GFP^+ cells in the inner and outer ML (iML and oML), respectively. **Each of these images was acquired in a z-stack at an interval of 0.2 μm, on average 15 slices per z stack.** For somatic analysis, images from 10 GFP^+ cell somas in the GCL were taken per animal. **Each of the somatic images was acquired in a z-stack at an interval of 0.5 μm, on average 10-12 slices per z stack.** To ensure the lack of bias, dendrites and somas of all diameters were selected using the GFP channel only, by a researcher blind to the treatment conditions. **This was performed in a systematic manner by imaging in a medio-lateral direction starting with the supragranular blade.** For each ROI, confocal images were analyzed in ImageJ software (Sheffield,

2007), the brightness and contrast corrected **using the built-in ImageJ Auto function** and the noise reduced using the **Despeckle** functions. Spines were defined as protrusions from the dendritic shaft and were classified as filopodia (protrusion with long neck and no head), thin (protrusion with a neck and head < 0.6 μm in diameter), stubby (protrusion with no obvious neck or head), or mushroom spines (protrusion with a neck and a head with a diameter > 0.6 μm (Zhao, et al., 2006). Dendritic spine analysis included spine density (number of spines per μm) and classification of spine morphology. Synaptic proteins, recognized as $Cy3^+$ spherical clusters onto the GFP^+ dendrites, were analyzed in terms of cluster density (number of clusters per μm), cluster size (area in μm^2) and cluster localization (either on dendritic spine or on dendritic shaft) in the iML and oML, respectively. For somatic region, only the cluster density (number of clusters per μm^3) was evaluated. Co-localization of clusters on the GFP^+ dendrites or somas was confirmed by **both manual observation of each optical plane within a z-stack and orthogonal projections (see supplementary Fig. 1)**.

Quantification of gephyrin, NL-2, and $GABA_AR$-α2 expression on presumably mature neurons was performed using confocal microscopy. 4 ROIs engaging a representative part of the GCL ipsilateral to the LPS or vehicle injection (from -1.46 mm to -2.46 mm posterior to bregma) were analyzed per animal. The images were then imported into ImageJ software (NIH, USA) and the mean gray value was measured per ROI. Background intensity was measured from corresponding stained sections in which primary antibody was omitted. This value was then subtracted from the mean gray value from each of the 4 ROIs in order to obtain a background-corrected mean gray value per animal.

Statistical analysis

All comparisons were performed using unpaired Student's t-test unless stated otherwise. Two-way analysis of variance (ANOVA) followed by a Bonferroni *posthoc* test was used for analyzing the microglial morphology and ELISA data. Non-parametric Mann-Whitney test was used for analyzing the NL-2 data in addition to Student's t-test. Data are presented as means±SEM, and differences considered significant at $p<0.05$.

Results

Lipopolysaccharide (LPS)-induced hippocampal inflammation exhibits a distinct acute, sub-acute, and long-lasting profile

We have previously performed intra-cortical and -hippocampal LPS injections when studying the effect of inflammation on the proliferation, differentiation and synaptic transmission of newly formed hippocampal neurons *born into an* ***inflammatory*** environment (Ekdahl, et al., 2003, Jakubs, et al., 2008). In the present study, we were interested in understanding how newly formed hippocampal neurons *born in an intact* environment may react to an LPS-induced inflammatory response at different synaptic developmental stages. Since the newborn neurons would now encounter both the acute, sub-acute, and late phases of LPS-induced inflammation, we first performed a more detailed temporal description of the pathological environment following a single hippocampal LPS injection. This included countings and

morphological evaluations of surveying and activated microglial cells, as well as measurements of pro- and anti-inflammatory cytokines at three representative time points. **Injection coordinates and LPS doses were evaluated in pilot experiments (see supplementary results).**

We examined the microglial response within the ipsilateral dorsal dentate gyrus at 12 h, 3-5 days and 3 weeks post-LPS injection (Fig. 1A-D). At 12 h, the number of Iba1/ED1 double-labeled ($Iba1^+/ED1^+$) cells was significantly higher in the ML in the LPS compared to the vehicle group (Fig. 1E). There were no changes in the SGZ/GCL (Fig. 1E) or in the dentate hilus (vehicle 24.92±0.22 vs LPS 30±3 cells per section). Morphologically, there was a significant increase in the percentage of round/amoeboid $Iba1^+$ cells, representing an activated microglial phenotype, in the ML (Fig. 1F) and the SGZ/GCL (Fig. 1G), while this increase did not reach significance in the dentate hilus (ramified: vehicle 11.67±5.36 vs LPS 4.17±0.68, intermediate: vehicle 83.33±3.85 vs LPS 75±1.36, round/amoeboid: vehicle 5±1.67 vs LPS 20.83±2.04) (**see supplementary Fig. 2 for representative images of the different microglial phenotypes**). At 3-5 days, we continued to observe increased numbers of $Iba1^+/ED1^+$ cells in the ML (Fig. 1H), while there were no changes in the SGZ/GCL (Fig. 1H) or in the dentate hilus (vehicle 20.47±0.8 vs LPS 22.08±1.34 cells per section). Morphologically, we found a reduction in the percentage of ramified surveying $Iba1^+$ cells together with a profound increase in the percentage of intermediate activated $Iba1^+$ cells in both the ML (Fig. 1I) and the SGZ/GCL (Fig. 1J). In the hilus, only the decrease in the percentage of ramified cells reached significance (ramified: vehicle 20.88±1.30 vs LPS 7.78±0.55; $p<0.05$, intermediate: vehicle 72.16±1.52 vs LPS 78.33±3.47; $p>0.05$, round/amoeboid: vehicle 6.96±0.29 vs LPS 13.89±2.94; $p>0.05$). At 3 weeks after LPS injection, there

was still a significant increase in the number of $Iba1^+/ED1^+$ cells within the ML (Fig. 1K), while no changes were observed in the SGZ/GCL (Fig. 1K) or in the dentate hilus (vehicle 24.62±1.89 vs LPS 28±2.47 cells per section). When comparing the morphology of microglial cells, a significant decrease was also observed in the percentage of ramified surveying $Iba1^+$ cells, with a concomitant increase in the percentage of intermediate activated $Iba1^+$ cells in both the ML (Fig. 1L) and the SGZ/GCL (Fig. 1M), with no changes in the dentate hilus (ramified: vehicle 24.58±2.43 vs LPS 14.72±1.76, intermediate: vehicle 71.98±2.08 vs LPS 78.98±1.48, round/amoeboid: vehicle 3.44±0.94 vs LPS 6.3±0.98). Taken together, our findings show that a single intra-hippocampal LPS injection induces a strong activation of microglial cells that is sustained within the ML and the SGZ/GCL for at least 3 weeks.

Despite the marked degree of microglial activation, we did not detect any **differences in the overall cytoarchitecture of the dentate gyrus 3 weeks after an LPS compared to vehicle injection (see cresyl violet staining in supplementary Fig. 3A and B), and there was no difference in the GCL volume (vehicle 127.07±32.91 vs LPS 96.51±20.29 mm^3).** Densitometric analyses of the **representative areas within the ipsilateral GCL, ML and the dentate hilus at 3 weeks post-LPS injection (see supplementary Fig. 3C and D) could not reveal any significant increase in the activation of astrocytes in terms of GFAP intensity compared to vehicle controls (GCL; vehicle 11.77±2.56 vs LPS 11.74±1.92, ML; vehicle 9.08±2.31 vs LPS 13.03±4.40, Hilus; vehicle 17.44±3.85 vs LPS 27.04±3.81 mean pixel intensity).** Furthermore, no ongoing Fluoro-Jade positive neurodegeneration was observed in the dentate gyrus at 3 weeks following LPS injection (data not shown). This is in line with other reports (Herber, et al.,

2006), as well as our previous report in rats, where no Fluoro-Jade^{+} cells were visible either 1 or 8 weeks following a single intra-hippocampal LPS injection (Jakubs, et al., 2008).

We also assessed the magnitude of inflammation in the ipsilateral hippocampus in the acute (12 h), sub-acute (3 days) and late phase (3 weeks) following LPS injection by measuring the levels of pro- (IL-1β, IL-6) and anti-inflammatory (IL-4 and IL-10) cytokines using ELISA. At 12 h, there was an acute substantial increase in the expression of both IL-1β and IL-6 (Fig. 2A and B, respectively). The increase was transient and levels were non-detectable or comparable to vehicles already at 3 days post-LPS injection (Fig. 2A and B, respectively). Conversely, levels of both IL-4 (Fig. 2C) and IL-10 (Fig. 2D) did not differ between vehicle- and LPS-injected groups at any time point. However, their expression levels did follow a biphasic temporal response in the LPS-injected group with a significant reduction from 12 h to 3 days, followed by a significant increase from 3 days to 3 weeks (Fig. 2C and D). The lack of difference between the LPS and vehicle group at 3 days post-injection may be due to the high variation within the vehicle group.

New hippocampal neurons do not change their gross morphology when encountering LPS-induced inflammation during synaptic development

We next wanted to explore whether LPS-induced inflammation may alter the gross morphology of newborn hippocampal neurons at different developmental stages related to synapse formation. **Newly formed cells were labeled with GFP by stereotaxic intra-hippocampal injection of a retroviral vector (RV-GFP) that incorporates specifically into dividing cells (Jessberger, et al., 2007, van Praag,**

et al., 2002, Zhao, et al., 2006). Since we injected the RV-GFP at either 1 or 4 weeks before inducing the inflammatory response, and then waited 3 weeks before perfusion (28 dpi and 49 dpi, respectively), the initial proliferation and **1 or 4 week -** survival phase of the newly formed neurons occurred in an intact brain and were not affected by the LPS-induced inflammation. Instead, the pathological environment occurred either during the early or late phase of inhibitory and excitatory synapse formation (Ge, et al., 2008, Laplagne, et al., 2006). **At both these time points, the total number of surviving GFP$^+$ cells did not differ between treatment groups (28 dpi; vehicle 14.66±3.15 vs LPS 22±6.59, 49 dpi; vehicle 24.77±5.21 vs LPS 20.2±3.75). However, the GFP$^+$ cell counts should be interpreted with caution, keeping in mind the possible variations in retroviral transduction efficiency following stereotaxic intracerebral injections.** At 28 dpi, the majority of the GFP$^+$ cell bodies were oriented at a 90° angle in relation to the GCL in both vehicle- (Fig. 3A) and LPS-injected animals (Fig. 3B) (vehicle 64.57±3.05 vs LPS 65.40±3.88 %). Also, most of the GFP$^+$ cell bodies were located in the inner GCL (iGCL**; first one-third of the GCL**) with relatively few cells in the middle GCL (mGCL**; middle one-third of the GCL**) or outer GCL (oGCL**; last one-third of the GCL**) and almost none in the dentate hilus (Fig. 3C). However, we did observe a small decrease in the percentage of GFP$^+$ cells present in the iGCL, together with an increase in the percentage of cells in the mGCL, in the LPS-injected group (Fig. 3C). This change in migration pattern is in line with a previous study where newborn neurons formed in an LPS-induced inflammatory environment were reported to migrate a longer distance within the GCL compared to cells in control environment (Belarbi, et al., 2012), but the significance of this finding is not known. The dendritic tree was well extended into the oML in both groups, with frequent occurrence of small varicosities

on the dendrites indicating immature dendritic morphology (Fig. 3D), thereby corroborating prior findings (Jackson, et al., 2012, Toni, et al., 2007). The dendrites originated primarily from the apical side of the cell body and rarely from the medial or basal side, with no differences between the LPS- and vehicle-injected group (apical: vehicle 100±0 vs LPS 97.61±1.03, medial: vehicle 0±0 vs LPS 1.26±0.71, basal: vehicle 0±0 vs LPS 1.13±0.95 %). Also, no differences were observed between groups when estimating the percentage of basal (vehicle 81.55±3.73 vs LPS 91.15±2.91), medial (vehicle 12±1.93 vs LPS 7.80±2.6) and apical axons (vehicle 6.4±2.9 vs LPS 1.04±0.79).

At 49 dpi, most of the GFP^+ cell bodies were oriented at a 90° angle in relation to the GCL in both the vehicle- (Fig. 3E) and LPS-injected group (Fig. 3F) (vehicle 65.98±4.02 % vs LPS 62.38±3.27 %), which was similar to 28 dpi. The cell bodies were primarily located in the iGCL (Fig. 3G). The dendritic tree was now much more arborized than at 28 dpi, in both the groups, as previously reported for newborn hippocampal neurons of corresponding age (Jakubs, et al., 2008). Small varicosities were seldom observed (Fig. 3H). No differences were found between groups when estimating the percentage of apical (vehicle 92.27±1.98 vs LPS 90.45±2.53), basal (vehicle 2.56±1.10 vs LPS 5.17±1.82), or medial dendrites (vehicle 5.16±1.83 vs LPS 4.05±2.55). Also, similar findings were observed in the LPS- and vehicle-group regarding axonal origin at the cell body. Axons originated primarily from the basal (vehicle 70.23±5.69 % vs LPS 57.03±7.37 %) and medial side (vehicle 21.56±5.65 % vs LPS 25.52±4.98 %), and rarely from the apical side (vehicle 8.17±2.9 % vs LPS 7.51±3 %).

*Increased number of dendritic spines **and protein expression** at excitatory synapses on new hippocampal neurons encountering LPS-induced inflammation during early stages of synapse formation*

We investigated whether an LPS-induced inflammatory environment during either the early or late phase of synapse formation (28 dpi and 49 dpi, respectively) could selectively affect the excitatory synapses on newly formed hippocampal neurons. Dendritic spines are considered to be the main sites for excitatory synaptic input onto neurons, and can be divided into either immature phenotypes (filopodia and stubby spines), or mature phenotypes (thin and mushroom spines) (Nimchinsky, et al., 2002). At 28 dpi, all spine types were present on the new GFP^+ cells (Fig. 4A) with no significant differences between the LPS- and vehicle-group in spine density when data from the iML and oML were pooled together (Fig. 4B). However, when evaluating the two regions separately, we did detect a significant increase in the density of thin spines in the iML in the LPS-injected animals, **but not in the oML (Fig. 4C).** Conversely, at 49 dpi, LPS-induced inflammatory environment did not affect the spine density, neither when the iML and oML were pooled, nor when analyzed separately (iML: vehicle 0.73±0.1 vs LPS 0.54±0.08, oML: vehicle 0.79±0.08 vs LPS 0.72±0.07 spines/μm).

In an attempt to **substantiate** the increase in spine density during early synapse formation (28 dpi) **and correlate it** to a specific change at the excitatory synapses, we determined the expression of the post-synaptic excitatory scaffolding protein, PSD-95. PSD-95 is concentrated at glutamatergic synapses (El-Husseini, et al., 2000) and we have previously described its location on both dendritic spines and shafts of newborn hippocampal neurons (Jackson, et al., 2012). At 28 dpi, PSD-95 clusters were visible on the GFP^+ dendritic spines and shafts in the iML and oML in

both vehicle- (Fig. 4D) and LPS-injected animals (Fig. 4E) (vehicle 21.4± 5.1 vs LPS 23.8± 5.81 % clusters on spines), indicating that a substantial portion of the excitatory synapses were located on the dendritic shafts in both groups at this developmental stage. We found a trend towards an increase in the PSD-95 cluster density primarily on dendritic spines in the LPS-injected group, in both the iML and the oML (Fig. 4F). This was further supported by a small but significant increase in the size of the PSD-95 clusters present on dendritic spines in the oML **(Fig. 4G). No differences were present in the iML (Fig. 4G).**

We continued to examine the excitatory synapses at 28 dpi by quantifying the expression of the adhesion molecule N-cadherin. During development, N-cadherin is initially widely distributed within a cell, but becomes restricted primarily to the excitatory synapses as the cell matures (Benson and Tanaka, 1998). It has been shown to be involved in target recognition and synapse stabilization (Bamji, et al., 2003, Bozdagi, et al., 2004, Mendez, et al., 2010). At 28 dpi, N-cadherin clusters were present both on the dendritic spines and shafts of the GFP^+ new cells (Fig. 4H and I) (vehicle 16.1± 9.01 vs LPS 22.08± 7.57 % clusters on spines) with no differences between groups in either cluster density (iML: vehicle 0.02±0.009 vs LPS 0.01±0.004, oML: vehicle 0.02±0.011 vs LPS 0.02±0.008 cluster/μm) or cluster size (vehicle 0.11±0.018 vs LPS 0.09±0.017 μm^2) when clusters on spines and shafts were pooled together. Also, no differences were observed when the N-cadherin cluster density and size were evaluated separately on the dendritic spines of the newborn neurons (cluster density on spines- iML: vehicle 0.002± 0.002 vs LPS 0.003±0.002, oML: vehicle 0.003±0.002 vs LPS 0.006±0.004 cluster/μm; cluster size on spines- ML: vehicle 0.10±0.004 vs LPS 0.12±0.005 μm^2).

Nevertheless, we did observe co-localization of the N-cadherin clusters with PSD-95 (Fig. 4J).

***Alterations** at inhibitory synapses on new hippocampal neurons encountering LPS-induced inflammation during early stages of synaptic development*

We next wanted to explore possible changes at the inhibitory synapses on the newborn neurons following exposure to LPS at early and late phases of synapse formation. We, therefore, evaluated the expression of gephyrin, a post-synaptic scaffolding protein associated with clustering of $GABA_A$ and glycine receptors (Fritschy, et al., 2008). The gephyrin clusters were uniformly distributed in the somatic region of the GFP^+ cell bodies in both the vehicle- (Fig. 5A) and LPS-injected animals (Fig 5B). At 28 dpi, LPS-injected animals showed a significant decrease in the gephyrin cluster density in the somatic region (Fig. 5C). However, in the ML, where the gephyrin clusters were predominantly present on the dendritic shafts of GFP^+ neurons, as previously reported (Jackson, et al., 2012), neither the gephyrin cluster density (Fig. 5C) nor the size of the gephyrin cluster (vehicle 0.13±0.009 vs LPS 0.12±0.003 μm^2) were different between the groups. Also, at 49 dpi, no differences were observed in gephyrin cluster density in the GCL, iML, or oML (Fig. 5D) or in the size of the gephyrin clusters in the ML (vehicle 0.12±0.007 vs LPS 0.11±0.005 μm^2).

The LPS-induced decrease in gephyrin cluster density in the somatic region at 28 dpi could possibly reflect less inhibitory pre-synaptic input to the new neurons, leading to post-synaptic alterations (Chubykin, et al., 2007). We therefore assessed the number of GABA clusters on the GFP^+ cells at 28 dpi **as a measurement of pre-/peri-synaptic inhibitory input.** The distribution of GABA clusters was similar to

that of gephyrin in the somatic region (Fig. 5E). However, although we found co-localization of gephyrin and GABA clusters (Fig. 5F), there were no differences in GABA cluster density on GFP^+ cell soma between groups (vehicle 0.01±0.002 vs LPS 0.01±0.002 cluster/μm^3).

We then analyzed the expression of **post-synaptic** adhesion molecules known to regulate gephyrin clustering at inhibitory synapses. One of the most studied adhesion molecule at inhibitory synapses is the NL-2 (Hoon, et al., 2009), which drives the post-synaptic differentiation by directly binding to the gephyrin (Poulopoulos, et al., 2009). Consistently, we observed co-localization of NL-2 and GABA clusters (Fig. 5F), thereby confirming the localization of NL-2 at GABAergic inhibitory synapses. The distribution of NL-2 clusters was uniform throughout the GFP^+ cell body in the GCL (Fig. 5G and H) and on the dendritic shafts in the ML (Fig. 5I and J) in both vehicle- and LPS-injected animals, similar to the pattern for gephyrin. Interestingly, new neurons in the LPS group exhibited a significant increase in the NL-2 cluster density on the GFP^+ cell bodies in the GCL as well as on the dendritic shafts in the oML (Fig. 5K), together with a trend towards an increase also in the iML (vehicle 0.04±0.01 vs LPS 0.07±0.02, p =0.13). The size of the NL-2 clusters in the ML was unaltered (vehicle 0.12±0.004 vs LPS 0.13±0.006 μm^2). At 49 dpi, as for gephyrin, no changes were observed in the NL-2 cluster density in the GCL, iML, or oML (Fig. 5L) or in the size of the NL-2 clusters in the ML (vehicle 0.13±0.004 vs LPS 0.14±0.007 μm^2).

In order to confirm the NL-2 findings at 28 dpi, we investigated the expression of neurofascin, which is another adhesion molecule found at inhibitory synapses. It has previously been shown to have a specific stabilizing role at GABAergic synapses on the axon initial segment (AIS) (Kriebel, et al., 2011).

Neurofascin clusters were evenly distributed on the dendritic shafts of the GFP^+ cells in the iML and oML in both vehicle- and LPS-injected animals (Fig. 5M and N). Additionally, we observed neurofascin clusters in the somatic region and in the AIS of GFP^+ cells (Fig. 5O). Consistent with the NL-2 findings, neurofascin cluster density was increased in the ML at 28 dpi in the LPS group, both in the iML and oML (Fig. 5P). The size of the neurofascin clusters was unaltered (vehicle 0.11 ± 0.006 vs LPS 0.11 ± 0.005 μm^2).

The disproportionate alterations in scaffolding protein and adhesion molecule expression at inhibitory synapses at 28 dpi may be associated with alterations in post-synaptic GABAergic transmission, without corresponding changes in pre-/peri-synaptic GABA expression. We therefore analyzed $GABA_AR$-α2 expression, a GABA receptor subunit previously observed in new neurons at this developmental age (Wadiche, et al., 2005). The $GABA_AR$-α2 clusters were frequent and evenly distributed throughout the GFP^+ cell body at this developmental stage (Fig. 6A and B). Cluster density was significantly increased in the somatic region of GFP^+ cells exposed to the LPS treatment compared to controls (Fig. 6C).

Changes in gephyrin, NL-2, and $GABA_AR$-α2 expression are restricted to new neurons within the hippocampal granule cell layer

Densitometric analyses of representative areas within the ipsilateral GCL at 3 weeks post-LPS injection could not reveal any significant differences in the overall expression of gephyrin, NL-2, or $GABA_AR$-α2 (see supplementary Fig. 4). This may imply a selective vulnerability at inhibitory synapses on newborn neurons compared to mature granule cells.

Interleukin-1 type 1 receptor (IL-1R1) is expressed on newly formed hippocampal neurons

To gain further insight into the link between inflammatory mediators and synaptic proteins on new neurons, we assessed the distribution of one important pro-inflammatory cytokine receptor (IL-1 type 1 receptor (IL-1R1)) on the GFP^+ cells at 28 dpi. **We observed IL-1R1 clusters in both the LPS- and vehicle-injected group (Fig. 7A-C), but found no differences in IL-1R1 clusters density in the somatic region of new neurons between treatment groups (vehicle 0.017±0.003 vs LPS 0.019±0.004). Interestingly, densitometric analyses of representative areas revealed an un-even distribution within the dentate gyrus, with a significantly increased intensity in the GCL compared to the distal dendritic segments within the oML in the LPS group and a trend towards an increase in the vehicle group (Fig. 7D-F).** In addition, IL-1R1 was frequently found in close apposition to NL-2 clusters **(Fig. 7G and H)** and **occasionally** to PSD-95 **(Fig. 7I)**.

Discussion

Here, we demonstrate that adult-born hippocampal neurons *born in an intact* environment are susceptible to LPS-induced inflammation during their initial stages of synapse formation. The LPS-induced environment progressed through an acute pro-inflammatory profile towards a sub-acute and long-term activation of microglia, **without developing major changes in hippocampal cytoarchitecture, astrocytosis, or cell death.** During the 3 weeks of exposure to the LPS environment, new neurons developed normal gross morphology independently of

when the LPS environment was initiated, i.e. either 1 or 4 weeks after the cells had been formed. These findings are similar to our previous report on newly formed neurons *born into an inflammatory* environment (Jakubs, et al., 2008). However, here we found an increased number of dendritic thin spines and post-synaptic PSD-95 clusters on spines, on newly formed neurons exposed to the LPS environment during the early phase of synapse formation, i.e. 7-28 dpi. This coincided with a decreased post-synaptic clustering of gephyrin, but without an accompanying change in overall **pre-/peri-synaptic** GABAergic input. Interestingly, the expression of two adhesion molecules associated with inhibitory synapses, NL-2 and neurofascin, were both specifically increased **together with the post-synaptic $GABA_AR$-α2 expression** at this early time point.

The hippocampal immune response induced by a single intra-hippocampal LPS injection followed the classical phases of inflammation, with an initial transient increase in pro-inflammatory cytokines and a gradual increase in number of phagocytic microglia with an altered activated morphology. Consistent with our findings, microglia have been reported to remain activated for up to 4 weeks after a single intra-hippocampal injection of LPS in mice (Herber, et al., 2006). However, (Herber, et al., 2006) also presented an LPS-induced astrogliosis, which was not as evident in our study, probably due to the lower dose of LPS. **A relatively mild LPS-insult was here further supported by the lack of major changes in the cytoarchitecture of the hippocampus and absence of Fluoro-Jade-labeled cell death.** The rapid, several-fold increase in the expression of IL-1β and IL-6 at 12 h, which returned to either low or undetectable levels at 3 days and 3 weeks after LPS treatment, are in line with previous reports showing an acute increase in pro-inflammatory cytokine expression both in case of systemic (Terrando, et al., 2010) as

well as intra-cerebral (Nadeau and Rivest, 2002) LPS administration. In contrast, the anti-inflammatory cytokines IL-4 and IL-10 did not significantly differ between vehicle- and LPS-injected groups at any time point. Though, due to a high variation in the vehicle group, we cannot rule out a small decrease in IL-4 and IL-10 expression at 3 days post-LPS injection. Moreover, the biphasic temporal response among the LPS-injected animals is in line with a previous report in a model of controlled cortical impact injury where IL-4 showed a similar temporal expression profile (Dalgard, et al., 2012).

On the newly formed neurons, we found increased number of thin spines following intra-hippocampal LPS injection at 28 dpi, as previously reported on mature neurons at 4 weeks post-systemic LPS injection (Kondo, et al., 2011). The excessive number of spines, particularly during the initial stages of synaptogenesis, may reflect defects in synaptic pruning by the microglial cells. This hypothesis was recently presented in a study *in vivo* on CX3CR1-GFP mouse hippocampus where GFP^+ microglia were suggested to eliminate synaptic elements during the second and third postnatal weeks (Paolicelli, et al., 2011). Interestingly, in an independent study, CX3CR1 expression was down-regulated on microglial cells after systemic LPS treatment (Wynne, et al., 2010), which may indicate together with our findings that synaptic pruning and the number of spines could be related to the number of CX3CR1+ surveying microglia.

The LPS-induced increase in spine number and PSD-95 cluster density on spines may represent an enhanced excitatory synaptic connectivity in the newly formed neurons at their early stages of synaptogenesis. **In accordance, we have previously demonstrated an enhanced excitatory synaptic transmission in new hippocampal neurons born into an LPS-induced inflammatory environment**

(Jakubs, et al., 2008). In further support of this relationship, a decrease in spine number and PSD-95 clustering on spines at later stages of synaptic development in new neurons born after SE (Jackson, et al., 2012) has also been correlated to a decrease in excitatory transmission (Jakubs, et al., 2006). Previous studies have suggested an important role for N-cadherin during excitatory synaptic assembly and target recognition (Bamji, et al., 2003, Bozdagi, et al., 2004, Mendez, et al., 2010). Though, in the present study, the increase in spine density and PSD-95 clusters were not accompanied by an increase in the N-cadherin expression, neither on spines nor on dendritic shafts, which is similar to our previous report on new neurons post-SE (Jackson, et al., 2012). Together, these findings indicate that the level of **N-cadherin expression may not be sensitive to LPS-induced inflammation.** Instead, spine formation and the PSD-95 expression **may be more vulnerable** to different brain pathologies, but change differently depending on the age of the new neuron. **Whether these early synaptic alterations are transient or persistent during the lifespan of the cell remains to be elucidated.**

At the inhibitory synapses on newly formed neurons, the decrease in gephyrin was not accompanied by an overall change in GABA cluster density, suggesting no profound change in **pre/peri--synaptic inhibitory input**. Instead, we found an increase in the expression of NL-2 and neurofascin. This is in contrast to our previous finding (Jackson, et al., 2012), where new neurons formed after SE developed a transient decrease in NL-2 clusters and an increase in gephyrin in the iML at 6 weeks of age. One of the possible explanations for this discrepancy could be the time at which the newly formed neurons encountered a pathological insult. In the previous study on SE, new neurons were born in the seizure environment, as opposed to the present report where they were challenged with LPS-induced inflammation at

certain time windows after birth. However, the overall **disproportionate alterations** of adhesion molecule and scaffolding protein expression in both of these studies is likely to cause an imbalance in the inhibitory synaptic connectivity in the new hippocampal neurons. **Since the $GABA_AR$-α2 expression was increased in the present study, it could reflect an immature or perhaps dysfunctional GABAergic transmission in the new neurons, maybe associated with dispersion or altered clustering of $GABA_AR$-α2 at the inhibitory synapses, due to the relatively decreased levels of gephyrin (Kneussel, et al., 1999, Niwa, et al., 2012). Because these changes occur during the critical early period of synaptic development, when new neurons normally facilitate their survival and functional integration by using GABA signaling for proper establishment of the excitatory transmission (Dieni, et al., 2013), normal hippocampal function may be affected. Interestingly, new neurons have been demonstrated to contribute to hippocampal memory formation especially during their early development (Gu, et al., 2012, Kee, et al., 2007).**

Indeed, achieving the proper balance between excitation and inhibition (E/I balance), especially in the hippocampal dentate gyrus where there is a continuous production of newly formed neurons during adulthood, is important for the normal function of the hippocampal circuitry. This balance is maintained by an array of homeostatic mechanisms that regulate neuronal excitability (Turrigiano, 2011). One such mechanism is via coordinated expression of adhesion molecules (neuroligins and neurexins) and scaffolding proteins (PSD-95 and gephyrin) (Gkogkas, et al., 2013). For instance, knocking out the eukaryotic translation initiation factor 4E-binding protein 2 (eIF4E-BP2) in mice could lead to an increased expression of all neuroligins

without any change in the postsynaptic scaffolding proteins (Gkogkas, et al., 2013). These knockout mice exhibited increased ratio of excitatory to inhibitory synaptic inputs and an autistic-like phenotype. In line with these studies, we speculate that the disproportionate alterations in adhesion molecules and scaffolding proteins that we find here at inhibitory synapses may be related to dysfunctional neuronal synaptic connectivity in new neurons following the LPS treatment.

Several immune mediators have been shown to be important for synaptic transmission and neural plasticity (Yirmiya and Goshen, 2011). Pro-inflammatory cytokines including IL-1β, IL-6, and TNF-α increase excitatory synaptic transmission and/or decrease inhibitory synaptic transmission in the spinal cord (Kawasaki, et al., 2008). Furthermore, intra-cerebral application of IL-1β enhances seizure activity in experimental models of epilepsy (Vezzani, et al., 1999). Here, we found IL-1R1 expression on new neurons during normal conditions, according to previous studies (Koo and Duman, 2008), as well as following LPS-induced inflammation. The abundant close apposition between IL-1R1 clusters and NL-2 may suggest a direct interaction between IL-1 and the inhibitory synapses on newborn neurons. However, NL-2 cluster density is unaltered on 6 week-old hippocampal neurons in IL-1R1 knockout mice (Chugh D, Jackson J, Chapman K, Ekdahl CT, unpublished observation), though, changes may still be present during brain inflammation.

The current study, together with our previous reports on structural and functional integration of adult-born hippocampal neurons in pathological environments (Jackson, et al., 2012, Jakubs, et al., 2008, Jakubs, et al., 2006, Wood, et al., 2011), suggest an interaction between brain inflammation / microglial cells and inhibitory **synapses on new neurons, different from that of mature neurons.**

However, the interaction may even differ among certain populations of new neurons, i.e. between cells born before or after the brain insult and cells remaining in the GCL or migrating aberrantly into the dentate hilus (Ekdahl, 2012). In addition, the fraction of new neurons of different ages varies when proliferation and survival rate changes due to the brain pathology. Neurogenesis decreases following LPS-induced inflammation (Ekdahl, et al., 2003). Conversely, here no decrease in survival was observed, having in mind the caveats of comparing numbers of retrovirally transfected cells. Accordingly, new neurons born directly before the LPS insult may constitute a relatively large fraction of the total population of new neurons at a given time point following the LPS injection. However, whether the synaptic changes on these cells would be more relevant to the hippocampal function than alterations in new neurons born during the LPS-induced inflammation is not known.

In summary, our results provide the first evidence that LPS-induced inflammation in the brain induces post-synaptic **inhibitory and excitatory** changes during early phases of synaptogenesis in new hippocampal neurons. **They support the idea that synaptic adhesion molecules have an essential role in synaptic development.** Adhesion molecules at inhibitory synapses may be possible future therapeutic targets for modulation of neuronal synaptic transmission in neurological diseases.

Acknowledgements

This work was supported by the Swedish Research Council, ALF Grant for funding for medical training and research, O.E. and Edla Johanssons Scientific Foundation, Tore Nilson´s Foundation, and the Royal Physiographic Society in Lund.

Conflicts of interest

The authors declare that there are no conflicts of interest associated with this manuscript.

References

1. Arikkath, J., and Reichardt, L. F., 2008. Cadherins and catenins at synapses: roles in synaptogenesis and synaptic plasticity. Trends Neurosci 31**,** 487-494.
2. Arvidsson, A., Collin, T., Kirik, D., Kokaia, Z., and Lindvall, O., 2002. Neuronal replacement from endogenous precursors in the adult brain after stroke. Nat Med 8**,** 963-970.
3. Bamji, S. X., Shimazu, K., Kimes, N., Huelsken, J., Birchmeier, W., Lu, B., and Reichardt, L. F., 2003. Role of beta-catenin in synaptic vesicle localization and presynaptic assembly. Neuron 40**,** 719-731.
4. Belarbi, K., Arellano, C., Ferguson, R., Jopson, T., and Rosi, S., 2012. Chronic neuroinflammation impacts the recruitment of adult-born neurons into behaviorally relevant hippocampal networks. Brain Behav Immun 26**,** 18-23.
5. Bengzon, J., Kokaia, Z., Elmer, E., Nanobashvili, A., Kokaia, M., and Lindvall, O., 1997. Apoptosis and proliferation of dentate gyrus neurons after single and intermittent limbic seizures. Proc Natl Acad Sci U S A 94**,** 10432-10437.
6. Benson, D. L., and Tanaka, H., 1998. N-cadherin redistribution during synaptogenesis in hippocampal neurons. J Neurosci 18**,** 6892-6904.
7. Bozdagi, O., Valcin, M., Poskanzer, K., Tanaka, H., and Benson, D. L., 2004. Temporally distinct demands for classic cadherins in synapse formation and maturation. Mol Cell Neurosci 27**,** 509-521.

Formatted: English (U.S.)

8. Butovsky, O., Ziv, Y., Schwartz, A., Landa, G., Talpalar, A. E., Pluchino, S., Martino, G., and Schwartz, M., 2006. Microglia activated by IL-4 or IFN-gamma differentially induce neurogenesis and oligodendrogenesis from adult stem/progenitor cells. Mol Cell Neurosci 31**,** 149-160.

9. Chubykin, A. A., Atasoy, D., Etherton, M. R., Brose, N., Kavalali, E. T., Gibson, J. R., and Sudhof, T. C., 2007. Activity-dependent validation of excitatory versus inhibitory synapses by neuroligin-1 versus neuroligin-2. Neuron 54**,** 919-931.

10. Curtis, M. A., Eriksson, P. S., and Faull, R. L., 2007. Progenitor cells and adult neurogenesis in neurodegenerative diseases and injuries of the basal ganglia. Clin Exp Pharmacol Physiol 34**,** 528-532.

11. Dalgard, C. L., Cole, J. T., Kean, W. S., Lucky, J. J., Sukumar, G., McMullen, D. C., Pollard, H. B., and Watson, W. D., 2012. The cytokine temporal profile in rat cortex after controlled cortical impact. Front Mol Neurosci 5**,** 6.

12. Dalva, M. B., McClelland, A. C., and Kayser, M. S., 2007. Cell adhesion molecules: signalling functions at the synapse. Nat Rev Neurosci 8**,** 206-220.

13. Danton, G. H., and Dietrich, W. D., 2003. Inflammatory mechanisms after ischemia and stroke. J Neuropathol Exp Neurol 62**,** 127-136.

14. Deng, X. H., Ai, W. M., Lei, D. L., Luo, X. G., Yan, X. X., and Li, Z., 2012. Lipopolysaccharide induces paired immunoglobulin-like receptor B (PirB) expression, synaptic alteration, and learning-memory deficit in rats. Neuroscience 209**,** 161-170.

15. Dieni, C. V., Chancey, J. H., and Overstreet-Wadiche, L. S., 2013. Dynamic functions of GABA signaling during granule cell maturation. Front Neural Circuits 6.

16. Ekdahl, C. T., 2012. Microglial activation - tuning and pruning adult neurogenesis. Front Pharmacol 3**,** 41.

17. Ekdahl, C. T., Claasen, J. H., Bonde, S., Kokaia, Z., and Lindvall, O., 2003. Inflammation is detrimental for neurogenesis in adult brain. Proc Natl Acad Sci U S A 100**,** 13632-13637.

18. Ekdahl, C. T., Kokaia, Z., and Lindvall, O., 2009. Brain inflammation and adult neurogenesis: the dual role of microglia. Neuroscience 158**,** 1021-1029.

19. Ekdahl, C. T., Mohapel, P., Elmer, E., and Lindvall, O., 2001. Caspase inhibitors increase short-term survival of progenitor-cell progeny in the adult rat dentate gyrus following status epilepticus. Eur J Neurosci 14**,** 937-945.

20. El-Husseini, A. E., Schnell, E., Chetkovich, D. M., Nicoll, R. A., and Bredt, D. S., 2000. PSD-95 involvement in maturation of excitatory synapses. Science 290**,** 1364-1368.

21. Eriksson, P. S., Perfilieva, E., Bjork-Eriksson, T., Alborn, A. M., Nordborg, C., Peterson, D. A., and Gage, F. H., 1998. Neurogenesis in the adult human hippocampus. Nat Med 4**,** 1313-1317.

22. Fritschy, J. M., Harvey, R. J., and Schwarz, G., 2008. Gephyrin: where do we stand, where do we go? Trends Neurosci 31**,** 257-264.

23. Ge, S., Sailor, K. A., Ming, G. L., and Song, H., 2008. Synaptic integration and plasticity of new neurons in the adult hippocampus. J Physiol 586**,** 3759-3765.

24. Gkogkas, C. G., Khoutorsky, A., Ran, I., Rampakakis, E., Nevarko, T., Weatherill, D. B., Vasuta, C., Yee, S., Truitt, M., Dallaire, P., Major, F., Lasko, P., Ruggero, D., Nader, K., Lacaille, J. C., and Sonenberg, N., 2013.

Autism-related deficits via dysregulated eIF4E-dependent translational control. Nature 493**,** 371-377.

25. Gorter, J. A., Van Vliet, E. A., Aronica, E., Breit, T., Rauwerda, H., da Silva, F. H. L., and Wadman, W. J., 2006. Potential new antiepileptogenic targets indicated by microarray analysis in a rat model for temporal lobe epilepsy. J Neurosci 26**,** 11083-11110.

26. Gu, Y., Arruda-Carvalho, M., Wang, J., Janoschka, S. R., Josselyn, S. A., Frankland, P. W., and Ge, S., 2012. Optical controlling reveals time-dependent roles for adult-born dentate granule cells. Nat Neurosci 15**,** 1700-1706.

27. Herber, D. L., Maloney, J. L., Roth, L. M., Freeman, M. J., Morgan, D., and Gordon, M. N., 2006. Diverse microglial responses after intrahippocampal administration of lipopolysaccharide. Glia 53**,** 382-391.

28. Hoon, M., Bauer, G., Fritschy, J. M., Moser, T., Falkenburger, B. H., and Varoqueaux, F., 2009. Neuroligin 2 controls the maturation of GABAergic synapses and information processing in the retina. J Neurosci 29**,** 8039-8050.

29. Jackson, J., Chugh, D., Nilsson, P., Wood, J., Carlstrom, K., Lindvall, O., and Ekdahl, C. T., 2012. Altered synaptic properties during integration of adult-born hippocampal neurons following a seizure insult. PLoS One 7**,** e35557.

30. Jakubs, K., Bonde, S., Iosif, R. E., Ekdahl, C. T., Kokaia, Z., Kokaia, M., and Lindvall, O., 2008. Inflammation regulates functional integration of neurons born in adult brain. J Neurosci 28**,** 12477-12488.

31. Jakubs, K., Nanobashvili, A., Bonde, S., Ekdahl, C. T., Kokaia, Z., Kokaia, M., and Lindvall, O., 2006. Environment matters: synaptic properties of

neurons born in the epileptic adult brain develop to reduce excitability. Neuron 52, 1047-1059.

32. Jessberger, S., Zhao, C., Toni, N., Clemenson, G. D., Jr., Li, Y., and Gage, F. H., 2007. Seizure-associated, aberrant neurogenesis in adult rats characterized with retrovirus-mediated cell labeling. J Neurosci 27, 9400-9407.

33. Kawasaki, Y., Zhang, L., Cheng, J. K., and Ji, R. R., 2008. Cytokine mechanisms of central sensitization: distinct and overlapping role of interleukin-1beta, interleukin-6, and tumor necrosis factor-alpha in regulating synaptic and neuronal activity in the superficial spinal cord. J Neurosci 28, 5189-5194.

34. Kee, N., Teixeira, C. M., Wang, A. H., and Frankland, P. W., 2007. Preferential incorporation of adult-generated granule cells into spatial memory networks in the dentate gyrus. Nat Neurosci 10, 355-362.

35. Kneussel, M., Brandstatter, J. H., Laube, B., Stahl, S., Muller, U., and Betz, H., 1999. Loss of postsynaptic GABA(A) receptor clustering in gephyrin-deficient mice. J Neurosci 19, 9289-9297.

36. Kondo, S., Kohsaka, S., and Okabe, S., 2011. Long-term changes of spine dynamics and microglia after transient peripheral immune response triggered by LPS in vivo. Mol Brain 4.

37. Koo, J. W., and Duman, R. S., 2008. IL-1beta is an essential mediator of the antineurogenic and anhedonic effects of stress. Proc Natl Acad Sci U S A 105, 751-756.

38. Kriebel, M., Metzger, J., Trinks, S., Chugh, D., Harvey, R. J., Harvey, K., and Volkmer, H., 2011. The cell adhesion molecule neurofascin stabilizes axo-

Formatted: German (Germany)

axonic GABAergic terminals at the axon initial segment. J Biol Chem 286**,** 24385-24393.

39. Kubota, K., Inoue, K., Hashimoto, R., Kumamoto, N., Kosuga, A., Tatsumi, M., Kamijima, K., Kunugi, H., Iwata, N., Ozaki, N., Takeda, M., and Tohyama, M., 2009. Tumor necrosis factor receptor-associated protein 1 regulates cell adhesion and synaptic morphology via modulation of N-cadherin expression. J Neurochem 110**,** 496-508.

40. Laflamme, N., Echchannaoui, H., Landmann, R., and Rivest, S., 2003. Cooperation between toll-like receptor 2 and 4 in the brain of mice challenged with cell wall components derived from gram-negative and gram-positive bacteria. Eur J Immunol 33**,** 1127-1138.

41. Laplagne, D. A., Esposito, M. S., Piatti, V. C., Morgenstern, N. A., Zhao, C., van Praag, H., Gage, F. H., and Schinder, A. F., 2006. Functional convergence of neurons generated in the developing and adult hippocampus. PLoS Biol 4**,** e409.

42. Mendez, P., De Roo, M., Poglia, L., Klauser, P., and Muller, D., 2010. N-cadherin mediates plasticity-induced long-term spine stabilization. J Cell Biol 189**,** 589-600.

43. Monje, M. L., Toda, H., and Palmer, T. D., 2003. Inflammatory blockade restores adult hippocampal neurogenesis. Science 302**,** 1760-1765.

44. Mosley, R. L., Hutter-Saunders, J. A., Stone, D. K., and Gendelman, H. E., 2012. Inflammation and Adaptive Immunity in Parkinson's Disease. Cold Spring Harbor Perspectives in Medicine 2.

45. Nadeau, S., and Rivest, S., 2002. Endotoxemia prevents the cerebral inflammatory wave induced by intraparenchymal lipopolysaccharide injection: role of glucocorticoids and CD14. J Immunol 169**,** 3370-3381.

46. Nguyen, M. D., Julien, J. P., and Rivest, S., 2002. Innate immunity: the missing link in neuroprotection and neurodegeneration? Nat Rev Neurosci 3**,** 216-227.

47. Nimchinsky, E. A., Sabatini, B. L., and Svoboda, K., 2002. Structure and function of dendritic spines. Annu Rev Physiol 64**,** 313-353.

48. Niwa, F., Bannai, H., Arizono, M., Fukatsu, K., Triller, A., and Mikoshiba, K., 2012. Gephyrin-Independent GABA(A)R Mobility and Clustering during Plasticity. Plos One 7.

49. Paolicelli, R. C., Bolasco, G., Pagani, F., Maggi, L., Scianni, M., Panzanelli, P., Giustetto, M., Ferreira, T. A., Guiducci, E., Dumas, L., Ragozzino, D., and Gross, C. T., 2011. Synaptic Pruning by Microglia Is Necessary for Normal Brain Development. Science 333**,** 1456-1458.

50. Parent, J. M., Yu, T. W., Leibowitz, R. T., Geschwind, D. H., Sloviter, R. S., and Lowenstein, D. H., 1997. Dentate granule cell neurogenesis is increased by seizures and contributes to aberrant network reorganization in the adult rat hippocampus. J Neurosci 17**,** 3727-3738.

51. Paxinos, G., and Watson, C., 1997. The rat brain in stereotaxic coordinates. Academic Press, Inc.

52. Poulopoulos, A., Aramuni, G., Meyer, G., Soykan, T., Hoon, M., Papadopoulos, T., Zhang, M. Y., Paarmann, I., Fuchs, C., Harvey, K., Jedlicka, P., Schwarzacher, S. W., Betz, H., Harvey, R. J., Brose, N., Zhang, W. Q., and Varoqueaux, F., 2009. Neuroligin 2 Drives Postsynaptic Assembly

at Perisomatic Inhibitory Synapses through Gephyrin and Collybistin. Neuron 63, 628-642.

53. Schmued, L. C., Albertson, C., and Slikker, W., Jr., 1997. Fluoro-Jade: a novel fluorochrome for the sensitive and reliable histochemical localization of neuronal degeneration. Brain Res 751, 37-46.

54. Sheffield, J. B., 2007. ImageJ, a useful tool for biological image processing and analysis. Microscopy and Microanalysis 13, 200-201.

55. Shichita, T., Sugiyama, Y., Ooboshi, H., Sugimori, H., Nakagawa, R., Takada, I., Iwaki, T., Okada, Y., Iida, M., Cua, D. J., Iwakura, Y., and Yoshimura, A., 2009. Pivotal role of cerebral interleukin-17-producing gammadeltaT cells in the delayed phase of ischemic brain injury. Nat Med 15, 946-950.

56. Spalding, K. L., Bergmann, O., Alkass, K., Bernard, S., Salehpour, M., Huttner, H. B., Bostrom, E., Westerlund, I., Vial, C., Buchholz, B. A., Possnert, G., Mash, D. C., Druid, H., and Frisen, J., 2013. Dynamics of hippocampal neurogenesis in adult humans. Cell 153, 1219-1227.

57. Terrando, N., Rei Fidalgo, A., Vizcaychipi, M., Cibelli, M., Ma, D., Monaco, C., Feldmann, M., and Maze, M., 2010. The impact of IL-1 modulation on the development of lipopolysaccharide-induced cognitive dysfunction. Crit Care 14, R88.

58. Thored, P., Heldmann, U., Gomes-Leal, W., Gisler, R., Darsalia, V., Taneera, J., Nygren, J. M., Jacobsen, S. E., Ekdahl, C. T., Kokaia, Z., and Lindvall, O., 2009. Long-term accumulation of microglia with proneurogenic phenotype concomitant with persistent neurogenesis in adult subventricular zone after stroke. Glia 57, 835-849.

Formatted: English (U.S.)

59. Toni, N., Teng, E. M., Bushong, E. A., Aimone, J. B., Zhao, C. M., Consiglio, A., van Praag, H., Martone, M. E., Ellisman, M. H., and Gage, F. H., 2007. Synapse formation on neurons born in the adult hippocampus. Nat Neurosci 10**,** 727-734.

60. Turrigiano, G., 2011. Too many cooks? Intrinsic and synaptic homeostatic mechanisms in cortical circuit refinement. Annu Rev Neurosci 34**,** 89-103.

61. Wadiche, L. O., Bromberg, D. A., Bensen, A. L., and Westbrook, G. L., 2005. GABAergic signaling to newborn neurons in dentate gyrus. J Neurophysiol 94**,** 4528-4532.

62. van Praag, H., Schinder, A. F., Christie, B. R., Toni, N., Palmer, T. D., and Gage, F. H., 2002. Functional neurogenesis in the adult hippocampus. Nature 415**,** 1030-1034.

63. Washbourne, P., Dityatev, A., Scheiffele, P., Biederer, T., Weiner, J. A., Christopherson, K. S., and El-Husseini, A., 2004. Cell adhesion molecules in synapse formation. J Neurosci 24**,** 9244-9249.

64. Vezzani, A., Conti, M., De Luigi, A., Ravizza, T., Moneta, D., Marchesi, F., and De Simoni, M. G., 1999. Interleukin-1beta immunoreactivity and microglia are enhanced in the rat hippocampus by focal kainate application: functional evidence for enhancement of electrographic seizures. J Neurosci 19**,** 5054-5065.

65. Wood, J. C., Jackson, J. S., Jakubs, K., Chapman, K. Z., Ekdahl, C. T., Kokaia, Z., Kokaia, M., and Lindvall, O., 2011. Functional integration of new hippocampal neurons following insults to the adult brain is determined by characteristics of pathological environment. Exp Neurol 229**,** 484-493.

Formatted: German (Germany)

66. Wraith, D. C., and Nicholson, L. B., 2012. The adaptive immune system in diseases of the central nervous system. J Clin Invest 122**,** 1172-1179.

67. Wynne, A. M., Henry, C. J., Huang, Y., Cleland, A., and Godbout, J. P., 2010. Protracted downregulation of CX3CR1 on microglia of aged mice after lipopolysaccharide challenge. Brain Behav Immun 24**,** 1190-1201.

68. Yirmiya, R., and Goshen, I., 2011. Immune modulation of learning, memory, neural plasticity and neurogenesis. Brain Behav Immun 25**,** 181-213.

69. Yoshida, T., Shiroshima, T., Lee, S. J., Yasumura, M., Uemura, T., Chen, X. G., Iwakura, Y., and Mishina, M., 2012. Interleukin-1 Receptor Accessory Protein Organizes Neuronal Synaptogenesis as a Cell Adhesion Molecule. J Neurosci 32**,** 2588-2600.

70. Zhao, C., Deng, W., and Gage, F. H., 2008. Mechanisms and functional implications of adult neurogenesis. Cell 132**,** 645-660.

71. Zhao, C., Teng, E. M., Summers, R. G., Jr., Ming, G. L., and Gage, F. H., 2006. Distinct morphological stages of dentate granule neuron maturation in the adult mouse hippocampus. J Neurosci 26**,** 3-11.

72. Zhou, Y., Zhang, Y., Li, J., Lv, F., Zhao, Y., Duan, D., and Xu, Q., 2012. A comprehensive study on long-term injury to nigral dopaminergic neurons following intracerebroventricular injection of lipopolysaccharide in rats. J Neurochem 123**,** 771-780.

Figure legends

Figure 1. Lipopolysaccharide (LPS)-induced hippocampal inflammation exhibits an acute, sub-acute and long-lasting profile. A-D, Representative photomicrographs of the distribution of $Iba1^+$ (green), $ED1^+$ (red), and $Iba1^+$/ $ED1^+$ (yellow) microglia in the dentate gyrus after an intra-hippocampal vehicle injection (A), or 12 h (B), 3-5 days (C) or 3 weeks (D) after a LPS injection. Note the presence of ramified surveying microglia in vehicle group (arrowhead and inset in A), activated round/amoeboid microglia at 12 h post-LPS injection (arrowhead and inset in B), and activated microglia with an intermediate morphology at 3-5 days and 3 weeks post-LPS injection (arrowheads and insets in C and D, respectively). E-M, Quantifications showing the total number of $Iba1^+$/ $ED1^+$ microglia per section (E, H, and K) and the relative percentage of microglia with different morphological phenotypes (Ram – Ramified; Inter – Intermediate; R/A – Round / Amoeboid) in the ipsilateral molecular layer (ML) and granule cell layer (GCL) at 12 h (F and G), 3-5 days (I and J), and 3 weeks (L and M) post-LPS injection. Data are presented as mean±SEM, n=3 for each group (12 h), n=3 for each group (3-5 days), n=16 vehicle and n=18 LPS (3 weeks). *, $p<0.05$, 2-way ANOVA with Bonferroni *posthoc* test. Scale bar is 50 μm (in A for A, B, C, and D).

Figure 2. Several fold increase in pro-inflammatory cytokines acutely after intra-hippocampal LPS injection. A-D, Levels of interleukin (IL)-1β (A), IL-6 (B), IL-4 (C), and IL-10 (D) were measured at three different time points (12 h, 3 days, and 3 weeks post-LPS injection) in ipsilateral hippocampal lysate using ELISA. The levels of IL-1β and IL-6 were transiently increased 12 h after LPS compared to vehicle. Note also the transient significant decrease in levels of the anti-inflammatory

cytokines, IL-4 and IL-10, at 3 days compared to 12 h and 3 weeks post-LPS. Data are presented as mean±SEM, n=5 for each group (12 h), n=5 for each group (3 days), n=8 for each group (3 weeks). n.d. – not detectable. *, $p<0.05$, 2-way ANOVA with Bonferroni *posthoc* test.

Figure 3. New hippocampal neurons do not change their gross morphology when encountering LPS-induced inflammation during early and late phases of synaptic development. A-B, Photomicrographs representing the morphological development of GFP^+ newly formed cells in vehicle- (A) and LPS- (B) injected mice at 28 days post-injection (dpi). **Relative distribution of GFP^+ cell bodies in 3 sub-divisions of the GCL (inner, middle, outer GCL (iGCL, mGCL, and oGCL, respectively) are shown as insets in A (GFP^+ cell in the iGCL) and B (GFP^+ cell in the mGCL).** C, Quantification shows the relative distribution of GFP^+ cell bodies in **the** iGCL, mGCL, oGCL, or the dentate hilus. D, At 28 dpi, dendritic beading was clearly evident (arrowheads). E-F, Representative photomicrographs depict the morphological development of GFP^+ cells in vehicle- (E) and LPS- (F) injected mice at 49 dpi. Note the presence of highly branched dendritic tree extending into the outer ML (oML). G, Relative location of GFP^+ cells in the iGCL, mGCL, oGCL, or the dentate hilus. H, Dendritic beading was seldom observed at 49 dpi. Data are presented as mean±SEM, n=6 vehicle and n=8 LPS (28 dpi) and n=9 vehicle and n=10 LPS (49 dpi). *, $p<0.05$, unpaired t test compared to vehicle group. Scale bars are 50 μm (in A for A and B), 50 μm (in F for E and F), and 1 μm (in D for D and H).

Figure 4. Increased number of dendritic spines and subtle changes at excitatory synapses on new hippocampal neurons encountering LPS-induced inflammation

during early stages of synapse formation. A, Representative photomicrograph depicts different morphological subtypes of dendritic spines in relation to the dendritic shaft (DS). B, Spine density (pooled data from both inner ML (iML) and oML) on GFP^+ dendrites in vehicle- and LPS-injected animals. C, Note an increase in thin spine density in the iML in the LPS-injected group **and no changes in the oML**. D-E, Representative photomicrographs showing PSD-95 clusters in vehicle- (D) and LPS- (E) injected mice on a GFP^+ dendritic spine (arrow in E) and shafts (arrowheads in D and E). F, Cluster density of PSD-95 on GFP^+ dendritic spines in both iML and oML. G, Increased size of PSD-95 clusters present on GFP^+ dendritic spines in the oML **and no changes in the iML** in LPS-injected mice. H-I, Photomicrographs representing the expression of N-cadherin on GFP^+ dendritic spines and shafts (arrowheads) in vehicle- (H) and LPS- (I) injected mice. J, Photomicrograph showing the co-localization of N-cadherin (green) with PSD-95 (red) clusters (arrowheads). Also, single stained N-cadherin and PSD-95 clusters were present (arrows). Data are presented as mean±SEM, n=6-7 for each group (28 dpi). *, $p<0.05$, unpaired t test compared to vehicle group. Scale bars are 1 μm (A), 1 μm (in H for D, E, H, and I), and 1 μm (J).

Figure 5. Alterations at inhibitory synapses on new hippocampal neurons encountering LPS-induced inflammation during early but not later phases of synaptic development. A-B, Representative photomicrographs showing gephyrin expression in the somatic region of GFP^+ cells (arrowheads) in the vehicle- (A) and LPS- (B) injected mice at 28 dpi. C-D, Gephyrin cluster density was decreased in the GCL at 28 dpi (C), but no differences were observed between groups at 49 dpi (D). E, Image showing GABA clusters on GFP^+ cell soma (arrowheads) in vehicle-injected group

at 28 dpi. F, Photomicrographs showing the co-localization of GABA (green) and gephyrin (red) clusters (arrowhead in left panel) and that of GABA (green) and neuroligin-2 (NL-2) (red) clusters (arrowhead in right panel) in the ML, confirming the localization of gephyrin and NL-2 at inhibitory synapses. G-J, NL-2 expression on GFP^+ cell soma and dendritic shafts (arrowheads) in vehicle- (G and I, respectively) and LPS- (H and J, respectively) injected mice at 28 dpi. K-L, NL-2 cluster density was increased in the GCL and oML at 28 dpi (K), but no differences were found between groups at 49 dpi (L). M-N, Photomicrographs of neurofascin (NF) clusters on GFP^+ dendritic shafts (arrowheads) in vehicle- (M) and LPS- (N) injected mice at 28 dpi. O, Representative image from LPS-injected group showing expression of NF cluster on the GFP^+ cell soma (arrowhead) and axon initial segment (arrowhead in inset). P, Increased NF cluster density in the iML, and oML at 28 dpi. Data are presented as mean±SEM, n=6-7 for each group (28 dpi) and n=10 for each group (49 dpi). *, $p<0.05$, unpaired t test compared to vehicle group; #, $p<0.05$, Mann Whitney test compared to vehicle group. Scale bars are 1 μm (in A for A, B, E, G, and H), 1 μm (F), 1 μm (in I for I, J, M, and N), and 1μm (O).

Figure 6. LPS-induced increase in $GABA_AR$-α2 expression on new hippocampal neurons. A-B, Representative images showing $GABA_AR$-α2 labeling in the somatic region of GFP^+ cells (arrowheads) in vehicle- (A) and LPS- (B) injected mice. C, $GABA_AR$-α2 cluster density was increased on the GFP^+ cell soma in the GCL at 28 dpi. Data are presented as mean±SEM, n=3-4 for each group (28 dpi). *, $p<0.05$, unpaired t test compared to vehicle group. Scale bar is 1 μm (in A for A and B).

Figure **7**. IL-1 type 1 receptor (IL-1R1) is expressed predominantly at the somatic region of newly formed hippocampal neurons. A, Representative photomicrograph showing an overview of IL-1R1 expression on a GFP^+ cell in the GCL and ML of the dentate gyrus in an LPS-injected animal at 28 dpi. B-C, Orthogonal reconstructions from confocal z-series, viewed in x-z (**left**) and y-z (top) planes, showing the co-localization of IL-1R1 with a GFP^+ dendrite (arrowhead in B) and with a GFP^+ cell soma (arrowhead in C) marked as boxed regions in A. D-E, **Representative photomicrographs showing overall IL-1R1 expression in the GCL (D) and the oML (E) in LPS-injected mice. F, Increased expression of IL-1R1 in the GCL as compared to oML in LPS-injected group and a trend towards an increase in the vehicle group. G-H,** IL-1R1 clusters (green) in close apposition to NL-2 clusters (red) in the ML (arrowheads in **G**), confirmed with orthogonal projection (arrowhead in **H**). **I**, IL-1R1 clusters (green) in close apposition to PSD-95 clusters (red) in the ML (arrowheads). **Data are presented as mean±SEM, n=3-4 for each group (28 dpi). *, *p*<0.05, unpaired t test compared to vehicle group.** Scale bars are 10 μm (A and **in D for D and E**), 1 μm (B, in **G** for **G** and **H, and I**), and 2.5 μm (C)**.**

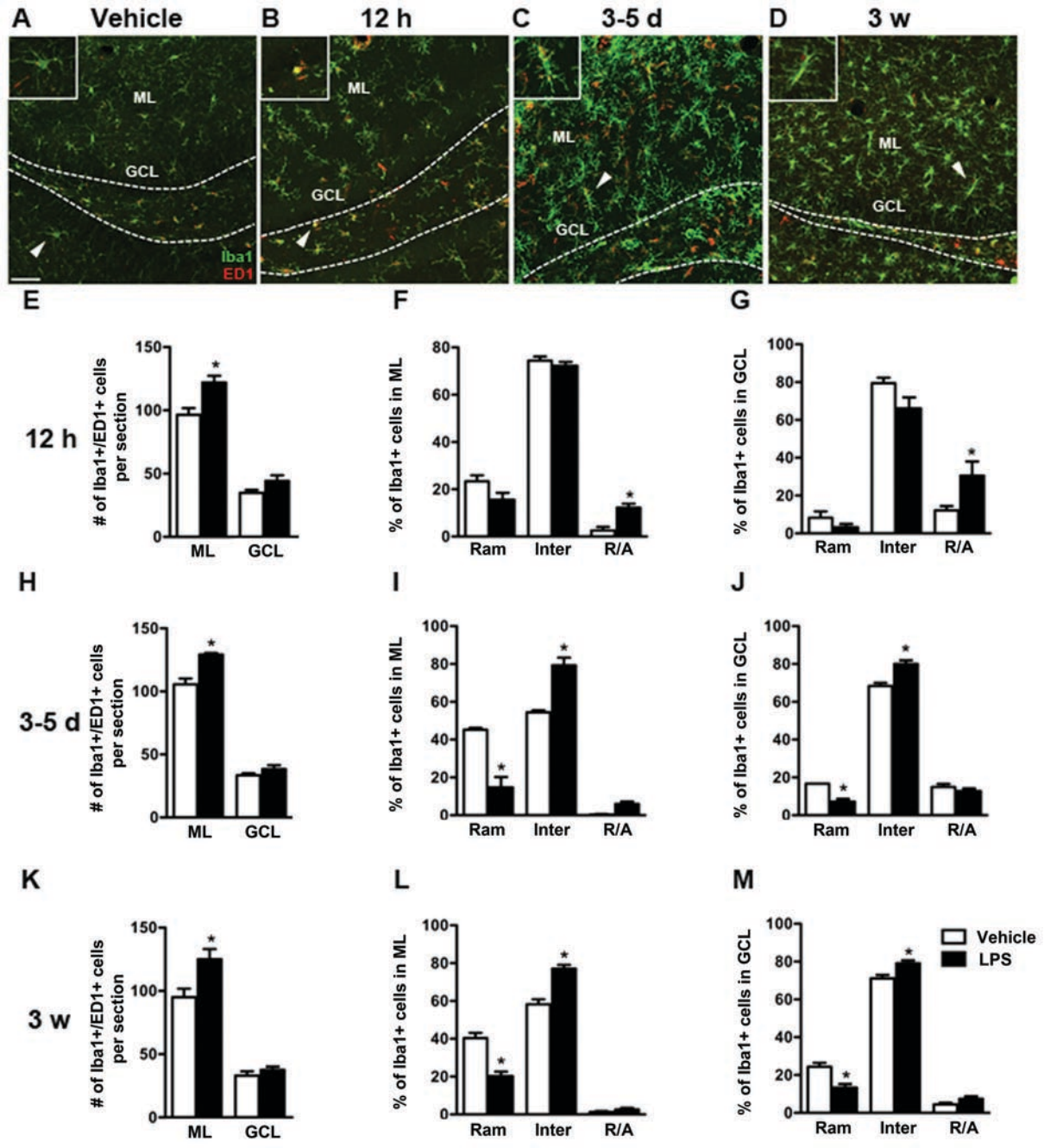
A
Vehicle
B
12 h
C
3-5 d
D
3 w
ML
GCL
Iba1
ED1
E
F
G
12 h
# of Iba1+/ED1+ cells per section
% of Iba1+ cells in ML
% of Iba1+ cells in GCL
ML
GCL
Ram
Inter
R/A
H
I
J
3-5 d
K
L
M
3 w
Vehicle
LPS

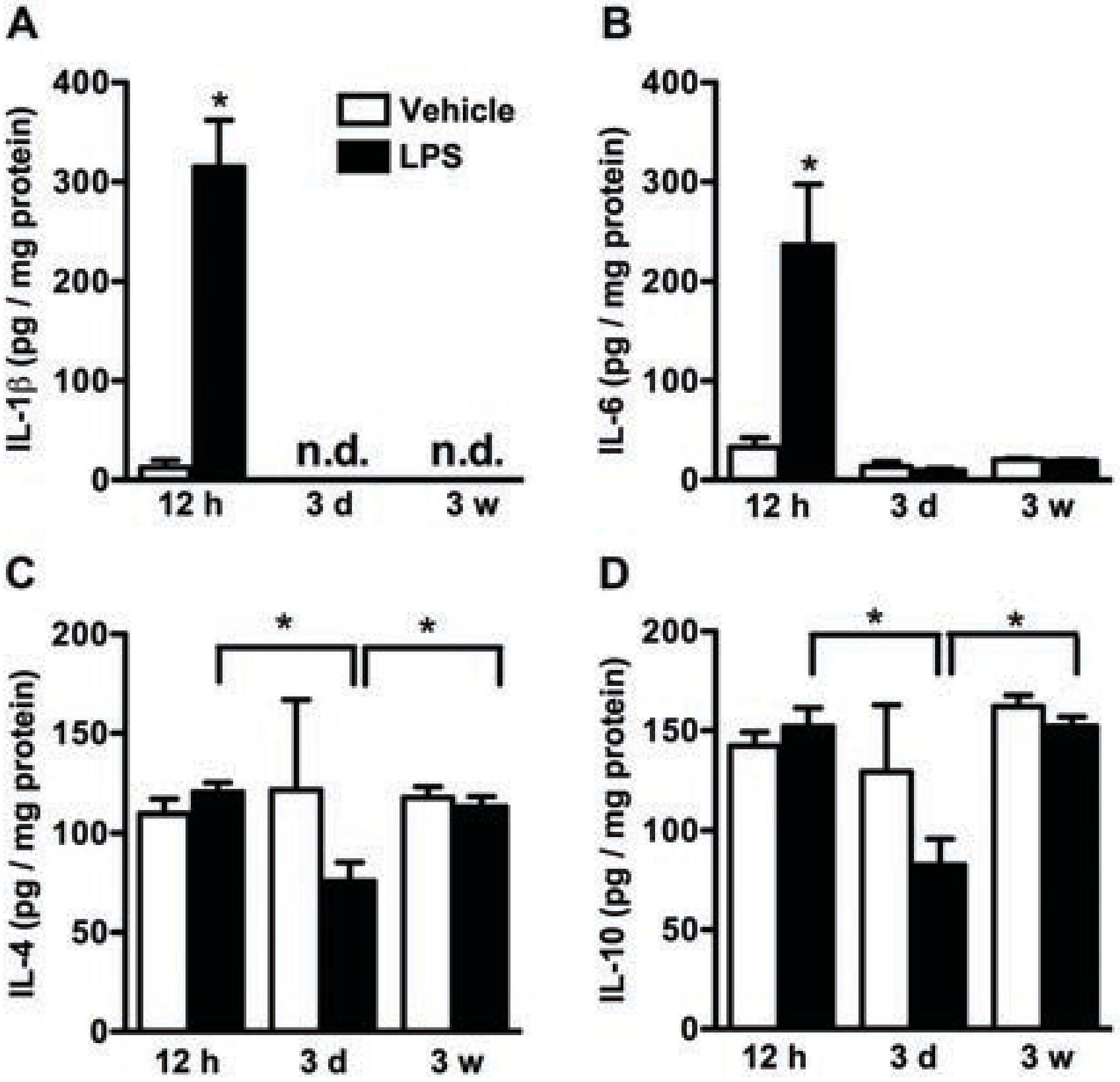
A
B
C
D
Vehicle
LPS
IL-1β (pg / mg protein)
IL-6 (pg / mg protein)
IL-4 (pg / mg protein)
IL-10 (pg / mg protein)
400
300
200
100
0
200
150
100
50
0
*
n.d.
n.d.
12 h
3 d
3 w

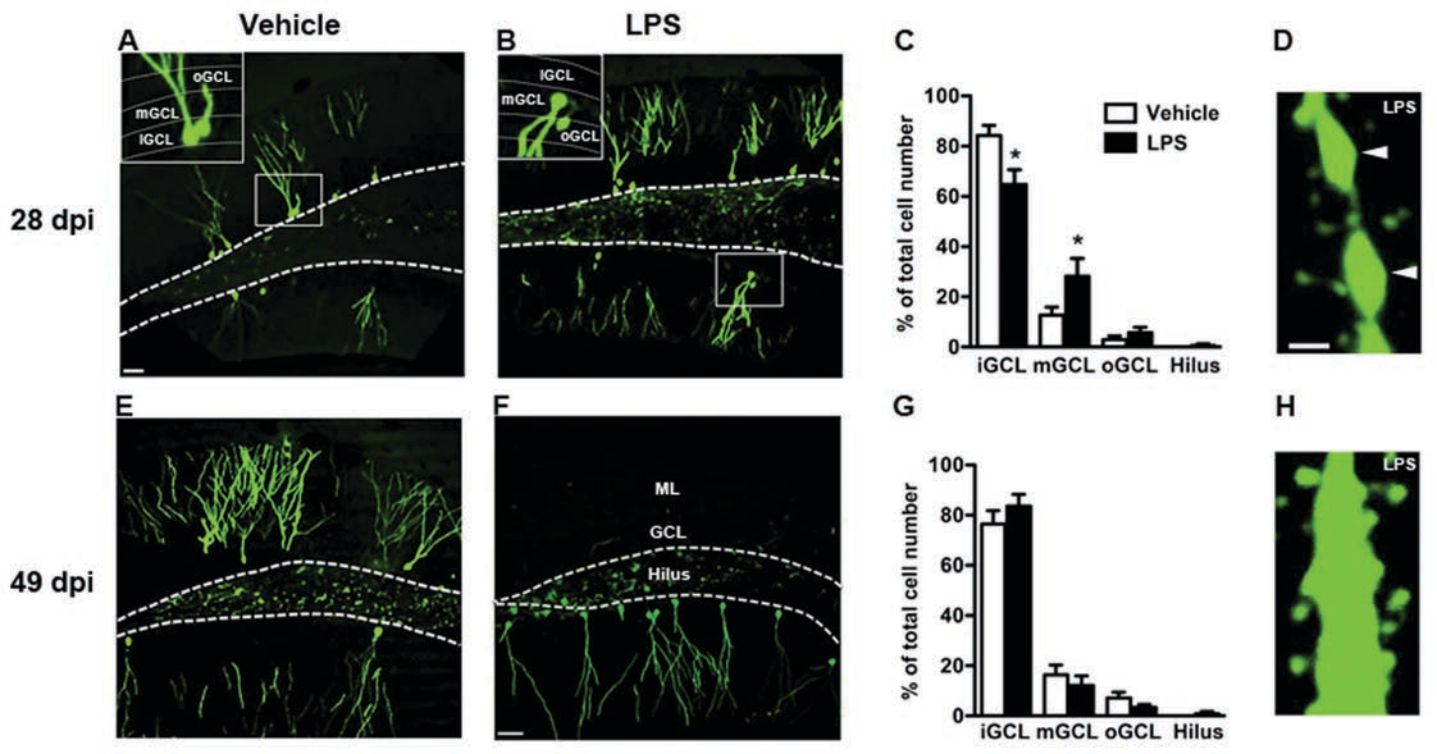
Vehicle
LPS
A
B
C
D
28 dpi
oGCL
mGCL
iGCL
iGCL
mGCL
oGCL
Vehicle
LPS
% of total cell number
100
80
60
40
20
0
iGCL mGCL oGCL Hilus
LPS
E
F
G
H
49 dpi
ML
GCL
Hilus
% of total cell number
100
80
60
40
20
0
iGCL mGCL oGCL Hilus
LPS

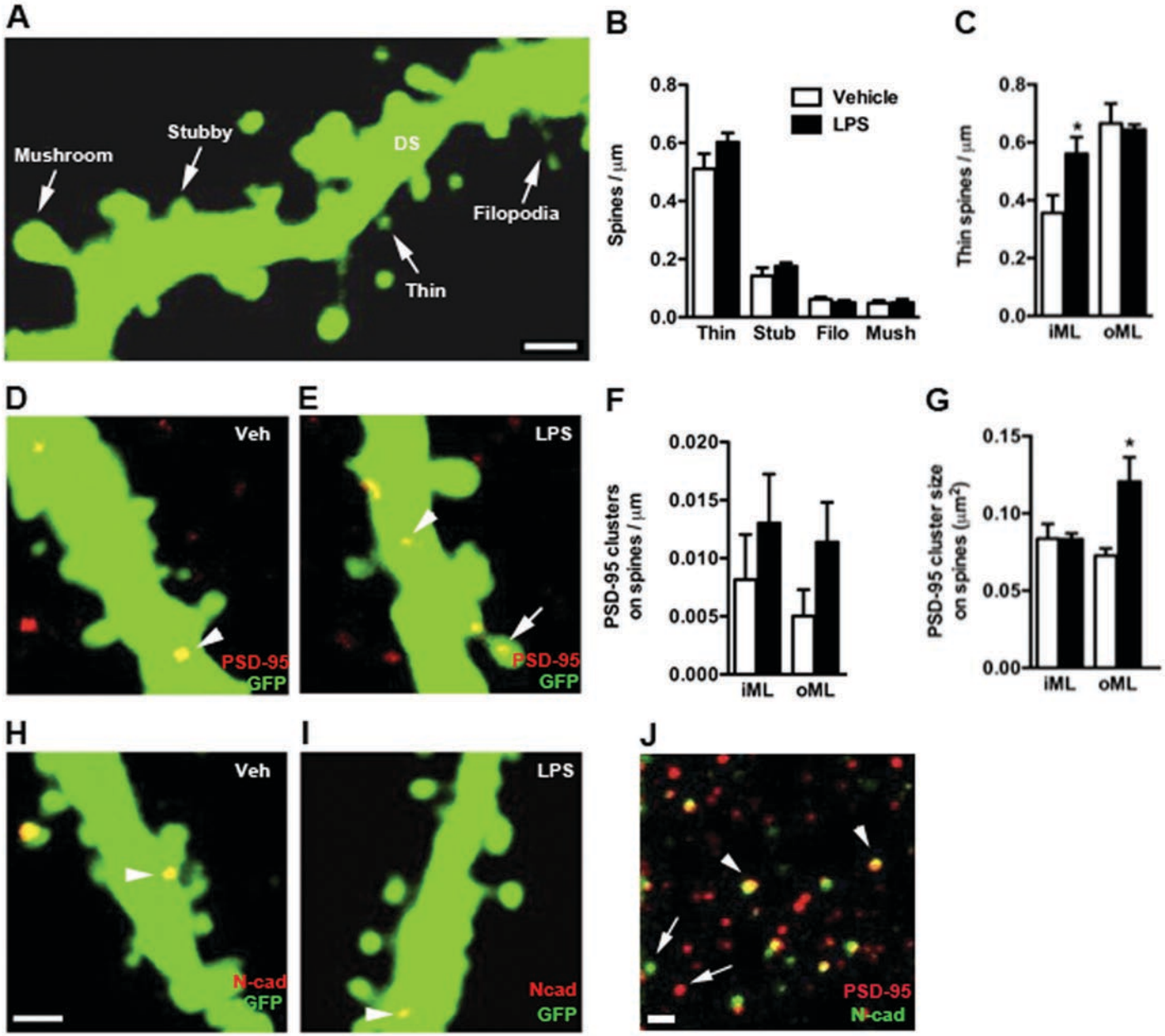
A
Mushroom
Stubby
DS
Filopodia
Thin
B
Spines / µm
0.8
0.6
0.4
0.2
0.0
Vehicle
LPS
Thin
Stub
Filo
Mush
C
Thin spines / µm
0.8
0.6
0.4
0.2
0.0
*
iML
oML
D
Veh
PSD-95
GFP
E
LPS
PSD-95
GFP
F
PSD-95 clusters on spines / µm
0.020
0.015
0.010
0.005
0.000
iML
oML
G
PSD-95 cluster size on spines (µm²)
0.15
0.10
0.05
0.00
*
iML
oML
H
Veh
N-cad
GFP
I
LPS
Ncad
GFP
J
PSD-95
N-cad

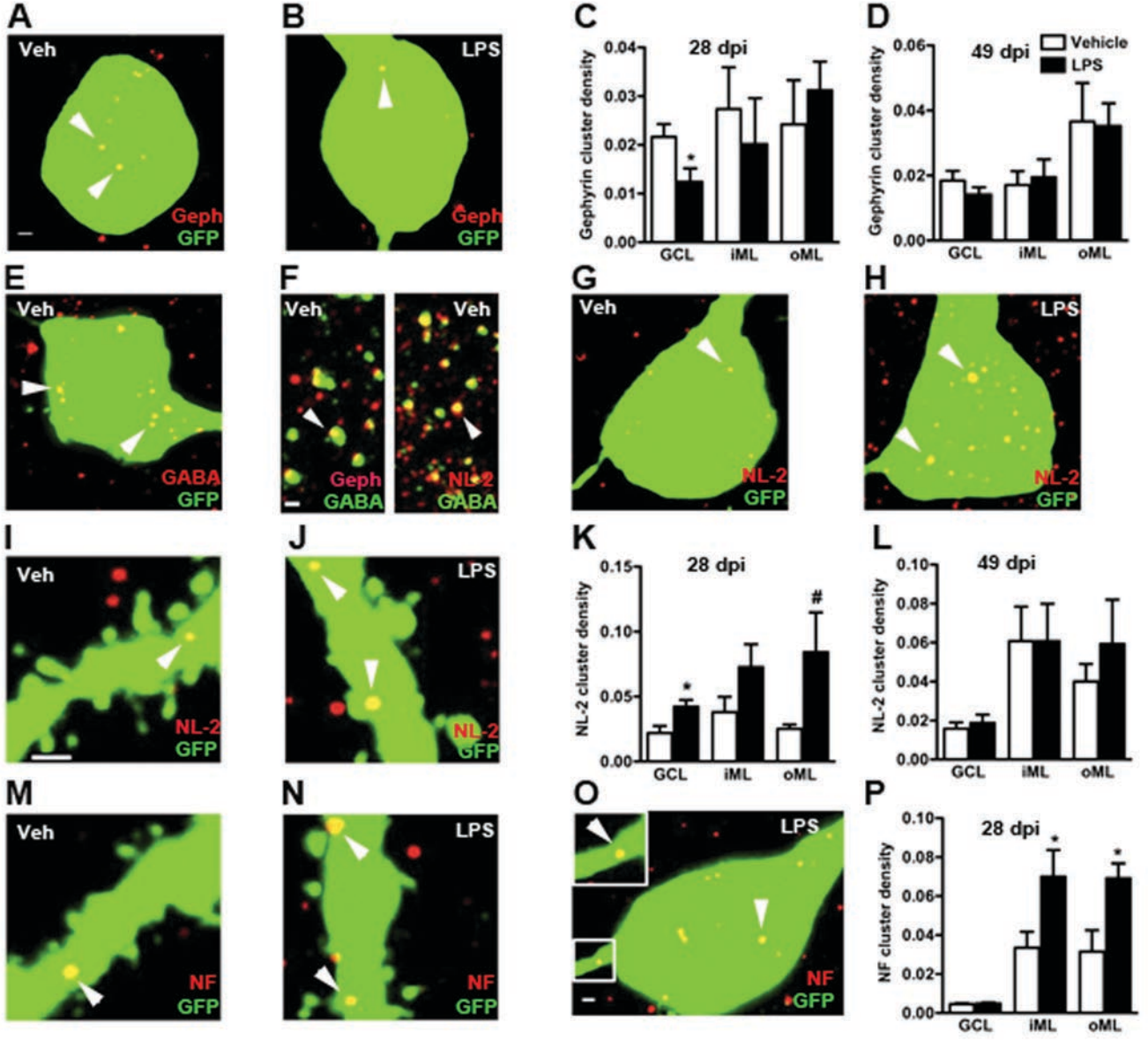
A
Veh
Geph
GFP
B
LPS
Geph
GFP
C
28 dpi
Gephyrin cluster density
0.04
0.03
0.02
0.01
0.00
*
GCL
iML
oML
D
49 dpi
Vehicle
LPS
Gephyrin cluster density
0.06
0.04
0.02
0.00
GCL
iML
oML
E
Veh
GABA
GFP
F
Veh
Geph
GABA
Veh
NL-2
GABA
G
Veh
NL-2
GFP
H
LPS
NL-2
GFP
I
Veh
NL-2
GFP
J
LPS
NL-2
GFP
K
28 dpi
NL-2 cluster density
0.15
0.10
0.05
0.00
*
#
GCL
iML
oML
L
49 dpi
NL-2 cluster density
0.10
0.08
0.06
0.04
0.02
0.00
GCL
iML
oML
M
Veh
NF
GFP
N
LPS
NF
GFP
O
LPS
NF
GFP
P
28 dpi
NF cluster density
0.10
0.08
0.06
0.04
0.02
0.00
*
*
GCL
iML
oML

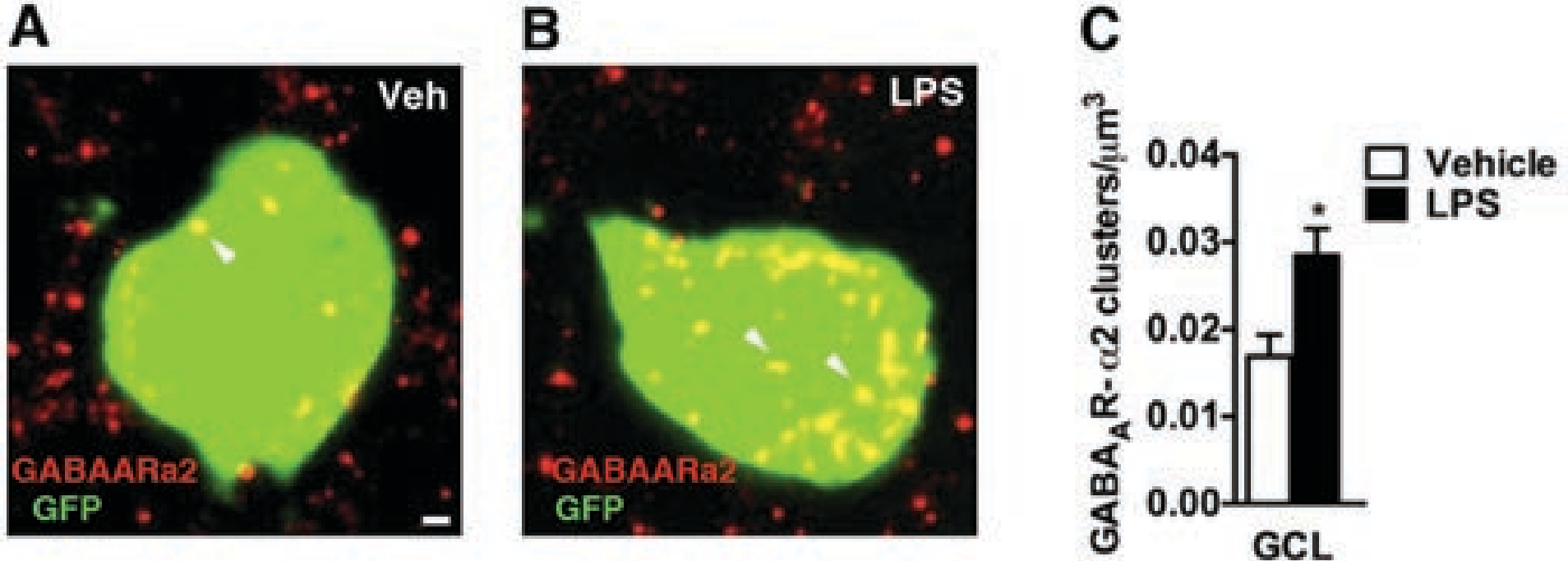
A
Veh
GABAARa2
GFP
B
LPS
GABAARa2
GFP
C
Vehicle
LPS
*
0.04
0.03
0.02
0.01
0.00
GABA$_A$R-α2 clusters/μm^3
GCL

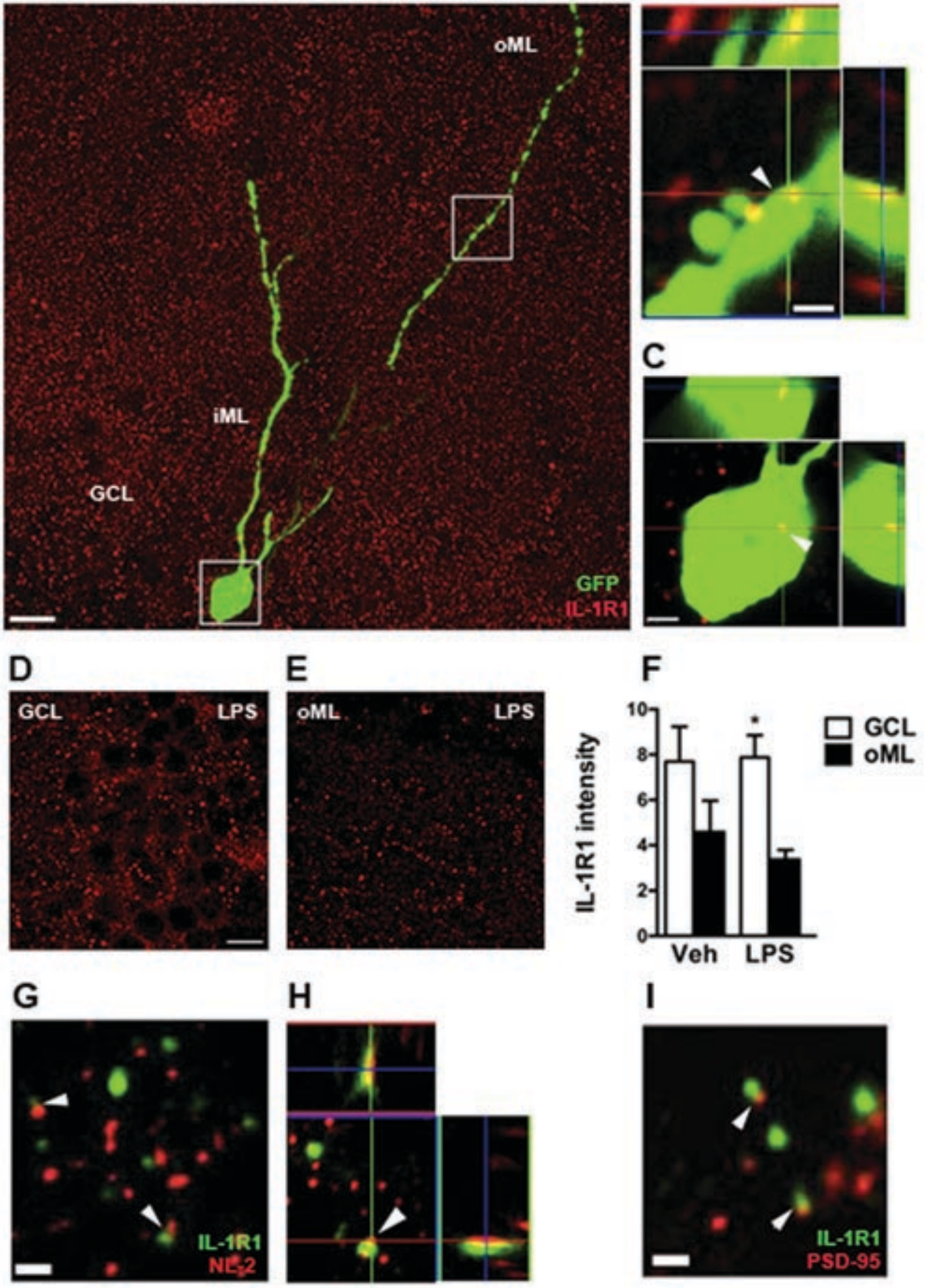
A
oML
iML
GCL
GFP
IL-1R1
B
C
D
GCL
LPS
E
oML
LPS
F
IL-1R1 intensity
10
8
6
4
2
0
*
GCL
oML
Veh
LPS
G
IL-1R1
NL2
H
I
IL-1R1
PSD-95

Supplementary Results

Optimization of the LPS dose and the coordinates for stereotaxic injection

In order to obtain a sustained inflammatory response in the ipsilateral dentate gyrus following a single LPS injection, we injected mice with 0.5 µl of 0.5 or 1 µg/µl LPS at two different intra-hippocampal coordinates and perfused them 3 days or 3 weeks later. Since we aimed for an inflammatory reaction primarily in the dorsal hippocampus, close to, but not at the same coordinates as that of the retroviral injection, without injecting directly into the dentate gyrus, coordinates for LPS injection within the dorsal CA1/CA3 region were chosen for the following experiments. We observed less microglial activation ($Iba1^+/ED1^+$ cells) within the ipsilateral dentate gyrus in the animals injected with 0.5 µl of 0.5 µg/µl LPS compared to 1 µg/µl, while the higher dose resulted in a sustained microglial activation throughout the dentate gyrus. We, therefore, decided to use the 1 µg/µl dose of LPS in the subsequent experiments.

Supplementary Figure Legends

Supplementary Figure 1. Representative photomicrographs of orthogonal reconstructions from confocal z-series, viewed in x-z (left) and y-z (top) planes, showing the expression of PSD-95 (A) and N-cadherin cluster (B) on GFP^+ dendrites, gephyrin (C) and GABA cluster (D) on GFP^+ cell soma, neuroligin-2 (E and F) on GFP^+ cell soma and dendrite, respectively, neurofascin (G and H) on GFP^+ cell soma and dendrite, respectively, and $GABA_AR$-α2 (I) on GFP^+ cell soma. Scale bar is 1 μm (in B for A, B, F, and H, in C, D, and E), 2 μm (G) and 5 μm (I).

Supplementary Figure 2. Microglia exhibit different morphological phenotypes depending on their activation state. A-C, Representative photomicrographs of three different morphological phenotypes observed during LPS-induced inflammation: ramified (A), intermediate (B) and round/amoeboid (C). Scale bar is 10 μm (in A for A, B, and C).

Supplementary Figure 3. No changes in cytoarchitecture of the hippocampal dentate gyrus and in glial fibrillary acidic protein expression (GFAP) due to LPS-induced inflammation compared to vehicle controls. A-B, Representative photomicrographs showing the dentate gyrus in cresyl violet staining 3 weeks following an ipsilateral intra-hippocampal vehicle- (A) or LPS-injection (B). C-D, Representative images of GFAP expression within the GCL, ML and hilus 3 weeks post-vehicle- (C) or LPS-injection (D). GCL; granule cell layer, ML; molecular layer, Hilus; dentate hilus. Dotted lines in A and B delineate the area of GCL used for volume estimations.

Squares in C represent the regions used for GFAP intensity measurements in the GCL, ML and hilus, respectively. Scale bar is 100 μm (in D for A, B, C and D).

Supplementary Figure 4. No LPS-induced alterations in expression levels of inhibitory synaptic proteins on presumably mature neurons. A-B, Representative photomicrographs showing gephyrin expression within the GCL 3 weeks following vehicle- (A) or LPS- (B) injection, 28 days post-retroviral injection. C, Quantification of gephyrin intensity values in the GCL. D-F, NL-2 expression in vehicle- (D) and LPS- (E) injected mice, and its quantification (F). G-I, $GABA_AR$-α2 expression in vehicle- (G) and LPS- (H) injected mice, and its quantification (I). Data are presented as mean±SEM, n=6-7 for each group (28 dpi). *, $p<0.05$, unpaired t test compared to vehicle group. Scale bar is 10 μm (in A for A, B, D, E, G, and H)

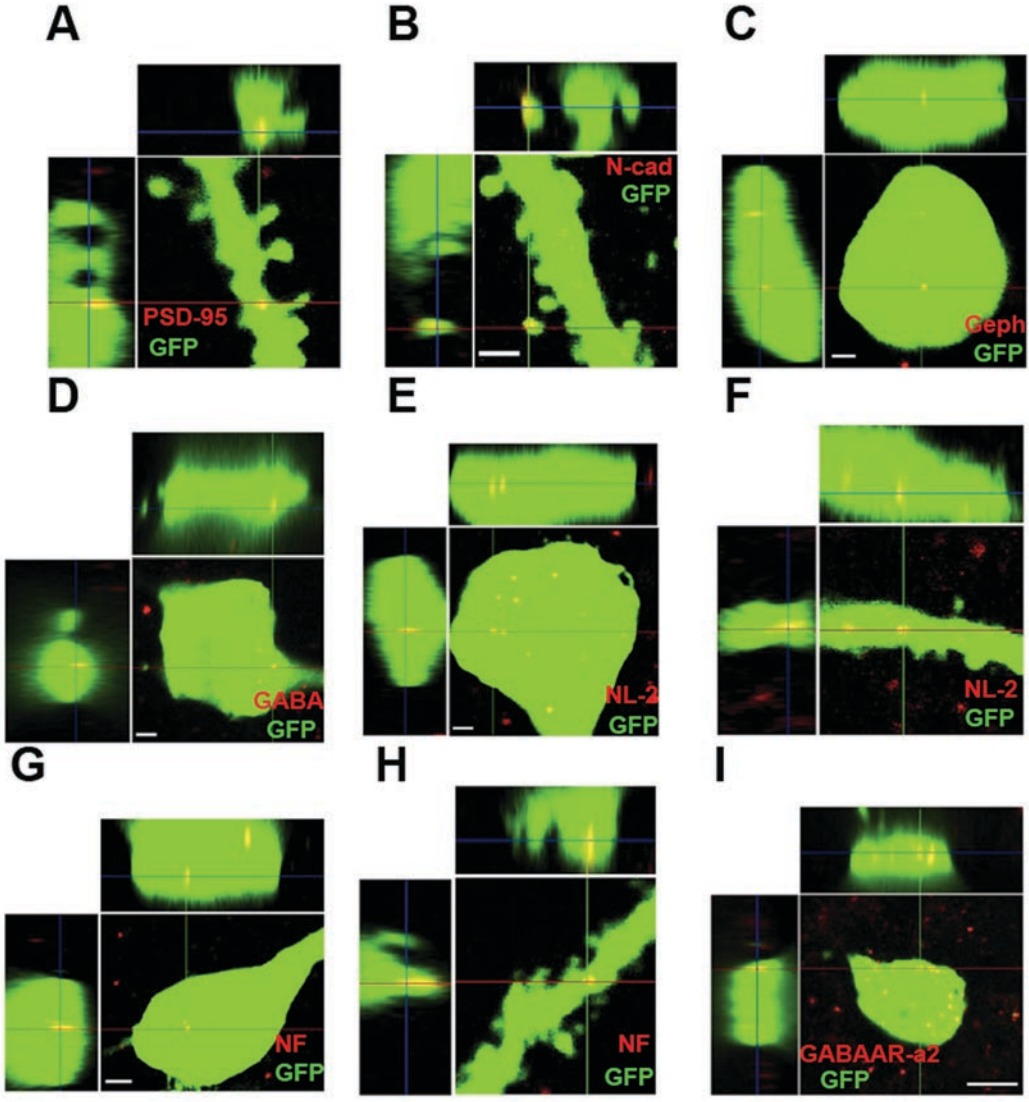
A
PSD-95
GFP
B
N-cad
GFP
C
Geph
GFP
D
GABA
GFP
E
NL-2
GFP
F
NL-2
GFP
G
NF
GFP
H
NF
GFP
I
GABAAR-a2
GFP

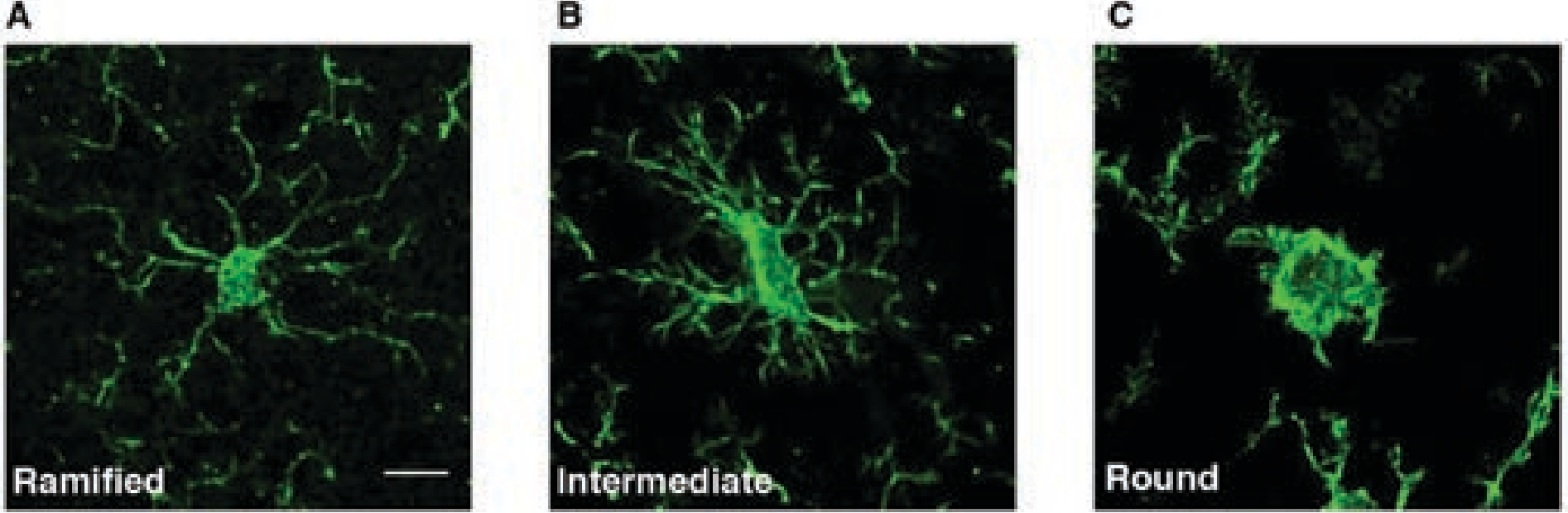
A
B
C
Ramified
Intermediate
Round

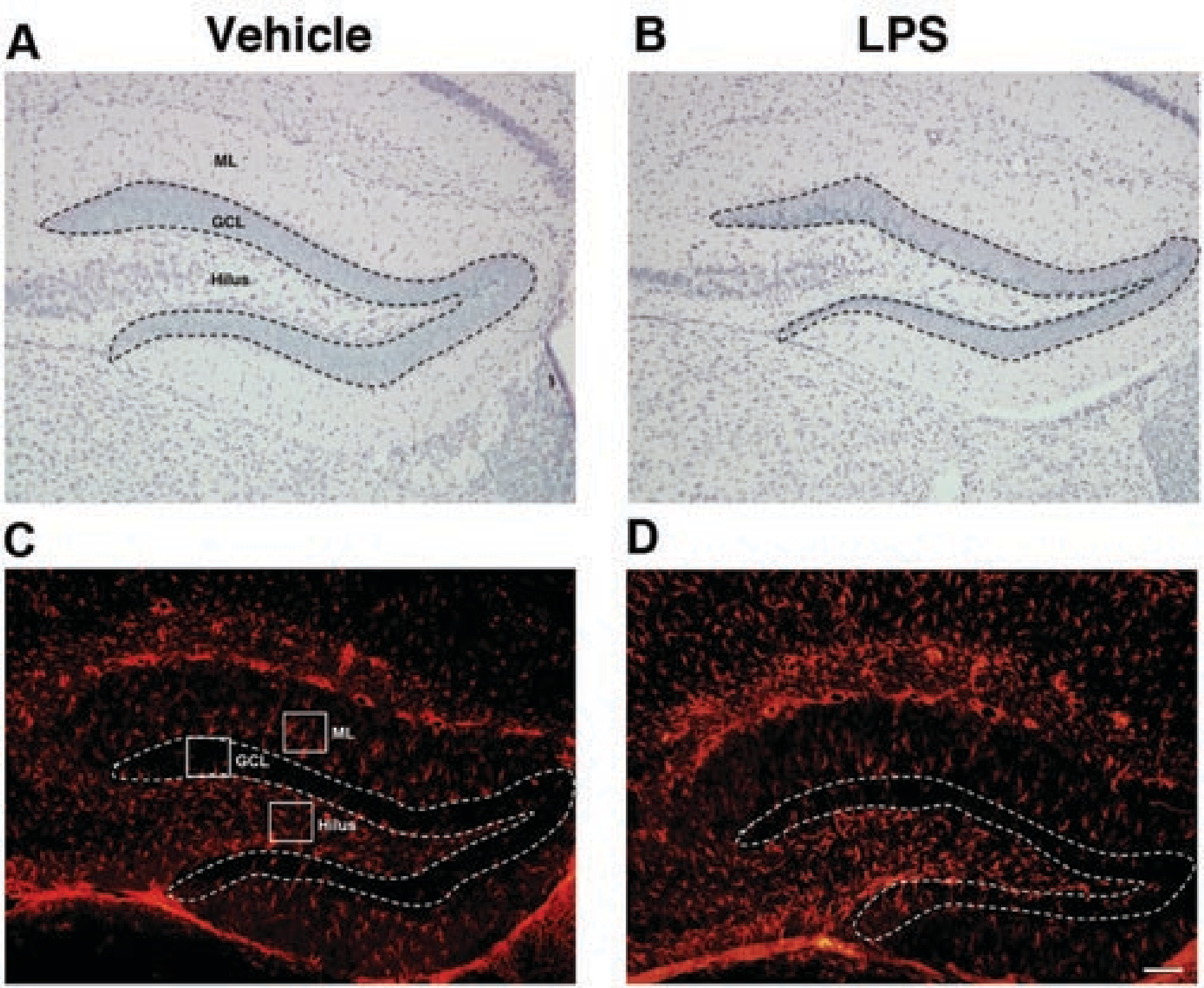
A
Vehicle
B
LPS
ML
GCL
Hilus
C
D
ML
GCL
Hilus

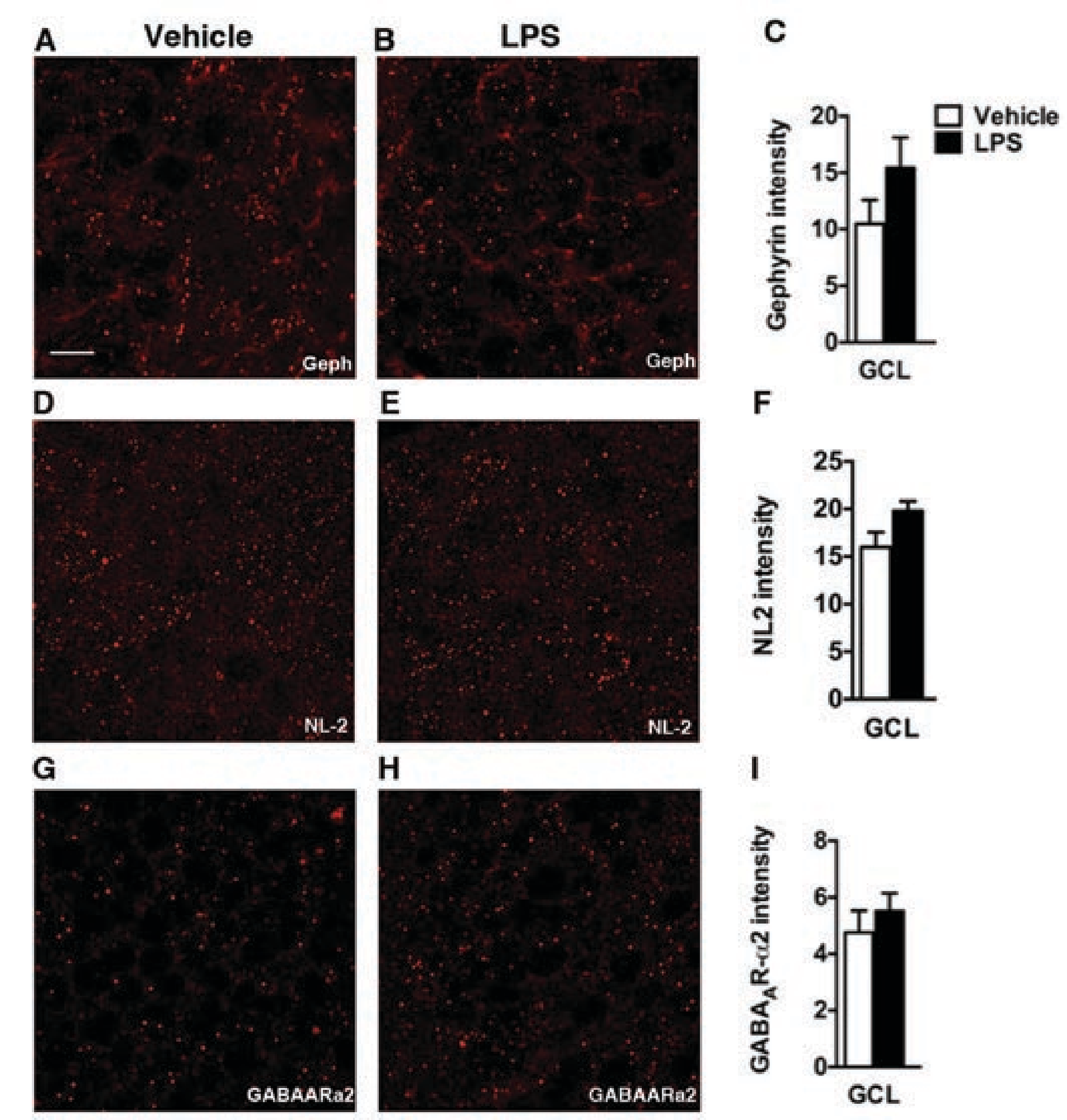
A
Vehicle
B
LPS
C
Geph
Geph
Vehicle
LPS
Gephyrin intensity
20
15
10
5
0
GCL
D
E
F
NL-2
NL-2
NL2 intensity
25
20
15
10
5
0
GCL
G
H
I
GABAARa2
GABAARa2
GABA$_A$R-α2 intensity
8
6
4
2
0
GCL